International Journal of Nanomedicine

Dovepress
open access to scientific and medical research

Open Access Full Text Article

ORIGINAL RESEARCH

Microcurrent Cloth-Assisted Transdermal Penetration and Follicular Ducts Escape of Curcumin-Loaded Micelles for Enhanced Wound Healing

Pei-Chi Lee[1,*], Cun-Zhao Li[2,*], Chun-Te Lu[3,4,*], Min-Han Zhao[2], Syu-Ming Lai[2], Man-Hua Liao[5], Cheng-Liang Peng[6], Hsin-Tung Liu[1], Ping-Shan Lai[2]

[1]xTrans Corporate Research and Innovation Center, Taipei City, Taiwan; [2]Department of Chemistry, National Chung Hsing University, Taichung, Taiwan; [3]Division of Plastic and Reconstructive Surgery, Department of Surgery, Taichung Veterans General Hospital, Taichung, Taiwan; [4]Institute of Medicine, School of Medicine, College of Medicine, National Yang Ming Chiao Tung University, Taipei, Taiwan; [5]Graduate Institute of Biotechnology, National Chung Hsing University, Taichung, Taiwan; [6]Isotope Application Division, National Atomic Research Institute, Taoyuan, Taiwan

*These authors contributed equally to this work

Correspondence: Ping-Shan Lai, Department of Chemistry, National Chung Hsing University, No. 145, Xingda Road, Taichung, 402, Taiwan, Tel +886-4-22840411 ext. 428, Fax +886-4-22862547, Email pslai@email.nchu.edu.tw

Purpose: Larger nanoparticles of bioactive compounds deposit high concentrations in follicular ducts after skin penetration. In this study, we investigated the effects of microcurrent cloth on the skin penetration and translocation of large nanoparticle applied for wound repair applications.

Methods: A self-assembly of curcumin-loaded micelles (CMs) was prepared to improve the water solubility and transdermal efficiency of curcumin. Microcurrent cloth (M) was produced by Zn/Ag electrofabric printing to facilitate iontophoretic transdermal delivery. The transdermal performance of CMs combined with M was evaluated by a transdermal system and confocal microscopy. The CMs/iontophoretic combination effects on nitric oxide (NO) production and inflammatory cytokines were evaluated in Raw 264.7 cells. The wound-healing property of the combined treatment was assessed in a surgically created full-thickness circular wound mouse model.

Results: Energy-dispersive X-ray spectroscopy confirmed the presence of Zn/Ag on the microcurrent cloth. The average potential of M was measured to be +214.6 mV in PBS. Large particle CMs (CM-L) prepared using surfactant/cosurfactant present a particle size of 142.9 nm with a polydispersity index of 0.319. The solubility of curcumin in CM-L was 2143.67 μg/mL, indicating 250-fold higher than native curcumin (8.68 μg/mL). The combined treatment (CM-L+M) demonstrated a significant ability to inhibit NO production and increase IL-6 and IL-10 secretion. Surprisingly, microcurrent application significantly improved 20.01-fold transdermal performance of curcumin in CM-L with an obvious escape of CM-L from follicular ducts to surrounding observed by confocal microscopy. The CM-L+M group also exhibited a better wound-closure rate (77.94% on day 4) and the regenerated collagen intensity was approximately 2.66-fold higher than the control group, with a closure rate greater than 90% on day 8 in vivo.

Conclusion: Microcurrent cloth play as a promising iontophoretic transdermal drug delivery accelerator that enhances skin penetration and assists CMs to escape from follicular ducts for wound repair applications.

Keywords: Zn/Ag electrofabrics, iontophoretic, self-assembly, anti-inflammatory agent, skin penetration, drug delivery

Introduction

Chronic wounds represent a significant burden to many people worldwide. The process of wound healing comprises several interconnected phases: hemostasis, inflammation, proliferation, maturation and remodeling.[1,2] Many advanced materials have been developed for wound repair that not only cover the wound but interact with it to promote wound

Received: 6 October 2023
Accepted: 6 December 2023
Published: 28 December 2023

healing through the formation of semi-permeable membranes, foams, hydrogels, hydrocolloids.[3] Several specific biomaterials used for deeper wounds form scaffolds to promote cell proliferation and provide mechanical support for tissue regeneration.[4] An integral element for healing is the initiation of an inflammatory response, which represents the foremost reaction subsequent to tissue damage.[5,6] The successful resolution of inflammation plays a pivotal role in preventing disease progression and expediting the healing process. However, impaired wound healing with dysfunctional immunoregulation can lead to stagnation in the inflammation phase. Delay in wound healing can be attributed to extensive inflammatory reactions, primarily instigated by bacterial infections. These infections subsequently instigate macrophage polarization failure and the irregular secretion of proinflammatory cytokines, including interleukin-1β (IL-1β), IL-6, and tumor necrosis factor-α (TNF-α).[7–9] Recently, several strategies have been explored to address chronic wounds by targeting the inflammatory microenvironment surrounding the wound vicinity. These strategies have included the use of steroids, nonsteroidal anti-inflammatory drugs (NSAIDs), cytokines, the introduction of naturally derived or synthetic scaffolds, and cell therapy.[10–14] Nonetheless, the side effects of steroids and NSAIDs, along with the risk of cytokine storms arising from excessive cytokine application, are concerns. Furthermore, the utilization of naturally derived or synthetic scaffolds, as well as cell therapy, can incur significant costs[15,16] while also facing the challenge of the skin barrier system, which imposes substantial limitations on the effective transport of active ingredients, consequently impeding the therapeutic efficacy of treatment.[17] Therefore, user-friendliness is necessary in developing a wound healing solution that is economical, has minimal side effects and adeptly addresses the hurdles presented by the skin barrier.

Curcumin (Cur, the chemical structure as shown in Figure 1), a herb extract from *curcuma longa*, has been widely used for medical purposes in Ayurveda and traditional Chinese medicine.[18] In recent decades, Cur has been studied extensively for its biofunctional properties, especially its anti-inflammatory, antioxidant, chemoprotective, tissue protective, antimicrobial, metabolism regulating, immuno-modulating, antineoplastic, and anti-depressant properties.[19–24] It can also act as an excellent wound healing agent to help rebuild damaged tissue by reducing inflammation and inducing cell proliferation.[25] Cur interacts with proinflammatory chemokines and cytokines, which are considered a major cause of inflammation during wound healing.[26] Additionally, it can enhance cutaneous wound healing by enhancing epithelial regeneration and increasing fibroblast proliferation, vascular density, and collagen deposition.[27] Although Cur exhibits excellent capabilities in the wound healing process, low water solubility and low bioavailability are major limitations for its biomedical application.[28]

It has been reported that topical application of Cur exhibits a greater wound healing effect than oral administration because Cur is more accessible and accumulates at the wound site.[29,30] Bioactive nanoparticles and nanocomposites have recently been demonstrated as potential applications to accelerate wound healing[31–33] using nanotechnology, including polymer-drug conjugates, polymer micelles, nanoparticles, composite particles, self-assembled lipid nanoparticles and liposomes for hydrophobic compounds delivery.[34–36] It is reported that Cur can be encapsulated in surfactant micelles to enhance its water solubility/dispersity.[37] Additionally, Cur nanoparticles with different sizes affect the therapeutic efficacy of curcumin. Average particles of 150 nm of Cur nanoparticles may escape uptake by phagocytes, and smaller particles can be efficiently internalized into cells and produce more pronounced therapeutic effects.[38,39]

In transdermal drug delivery (TDD) applications, the hair follicle route plays an important role in active ingredient penetration and storage. The follicular route is the preferred permeation pathway for nanoparticles and the penetration depth and capacity depend on particle size. Numerous animal models have validated that compounds in larger particles

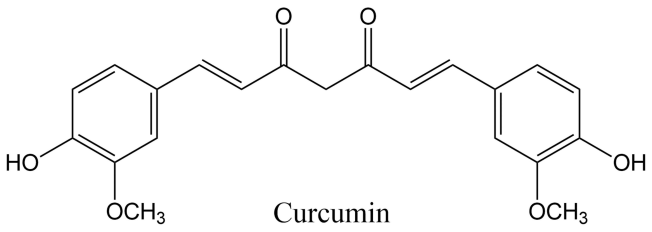

Figure 1 Chemical structure of curcumin.

could deposit high concentrations in follicular ducts and small amounts of compounds can be released from there by diffusion whereas small particles in the size range of 40 nm could be used to directly deliver bioactive compounds to specific cell populations, especially in barrier-compromised skin.[40,41] Thus, it is necessary to develop a strategy to facilitate the active compound release from follicular ducts after penetration.

Iontophoretic TDD systems drive the flow of charged molecules through microcurrents and simultaneously generate an electroosmotic flow of biological fluids for transdermal applications. These systems have been extensively studied.[42,43] When microcurrent is applied to skin tissue and cells, the number of organelles responsible for cell activities increases, thereby promoting cell proliferation and protein synthesis, which is considered to have potential wound healing applications.[44] Although iontophoretic TDD systems have been commercialized for topical skin analgesia, their large size, high cost, and complex energy storage power sources hinder their medical application.[45] Here, a microcurrent cloth was produced with printed silver (Ag) and zinc (Zn) electroceutical fabric, which can generate microcurrents without requiring extra equipment or batteries. Microcurrent cloth printed with Zn/Ag electroceutical fabric is considered to have potential for TDD and wound healing due to its antimicrobial activity and biocompatibility.[46–48]

In this study, Zn/Ag electrofabric-printed microcurrent cloth was produced to facilitate the skin penetration efficiency of Cur-loaded micelles (CMs). These fabrics can generate electricity for iontophoretic transdermal delivery without any additional equipment or charging. A self-assembly technique was applied to prepare CMs to improve water solubility and increase transdermal drug delivery efficiency. A Logan DHC-6T transdermal system equipped with the nonanimal artificial film Strat-M was used to conduct in vitro penetration experiments to verify the skin penetration ability of Cur in the micelle formulation. A surgically created full-thickness circular wound mouse model was established to further evaluate the wound repair ability of microcurrent cloth combined with a CMs formulation.

Materials and Methods

Materials

Cur (95% total curcuminoid content) was purchased from Alfa Aesar (Haverhill, MA, USA). Tween 20, Tween 80, and polyethylene glycol 400 (PEG 400) were purchased from Sigma–Aldrich (St. Louis, MO, USA), and Kolliphor RH40 was purchased from BASF (Ludwigshafen, Germany). Ag ink was purchased from Creative Materials Inc. (Ayer, MA, USA), and Zn particles (<10 μm) were purchased from Sigma Aldrich (St. Louis, MO, USA). Other chemicals were purchased from Sigma–Aldrich (St. Louis, MO, USA). The Strat-M membrane (Strat-M membrane, Trans dermal diffusion test model, 25 mm) was purchased from Millipore, Merck (Darmstadt, Germany). Lipopolysaccharide (LPS) was purchased from Sigma–Aldrich (Missouri, USA).

Murine macrophage Raw 264.7 cells (ATCC number: TIB-71™) were purchased from the American Type Culture Collection (ATCC, Virginia, USA). Raw 264.7 cells were cultured in Dulbecco's modified Eagle's medium (DMEM) supplemented with 1% penicillin–streptomycin-neomycin (PSN), 1% sodium pyruvate and 10% fetal bovine serum (FBS). All culture reagents were purchased from Invitrogen (Massachusetts, USA). Cells were maintained at 37°C under 5% CO_2.

Female 6-week-old BALB/c mice were purchased from LASCO Biotechnology (Co., Ltd, Taipei, Taiwan). The mice were housed in an air-conditioned animal room at 23±2°C and acclimated for 7 days before the experiments.

Preparation and Characterization of Microcurrent Cloth with Printed Zn/Ag Electroceutical Fabric

The in-house Zn/Ag ink prepared from a powder form was printed on the silk substrate to prepare Zn/Ag electrofabric-printed microcurrent cloth manufactured by xTrans Creative Inc. (Taipei, Taiwan) and the safety of Zn/Ag electrofabric-printed microcurrent cloth revealed a mean irritation index (M.I.I.) value of 0.07 that was considered non-irritant after an application for 48 consecutives hrs on 23 volunteers verified by SGS (kindly provided by xTrans Creative Inc.). Polyvinyl alcohol (PVA; Sigma Aldrich), a biocompatible binder, was used to hold the Zn particles in the ink and effectively adhere the particles to the supporting fabric during printing and curing.[49–51] The microstructure and EDX of the general cloth and Zn/Ag printed microcurrent cloth were determined using a field emission scanning electron microscope (FE-SEM; JSM-7800F, JEOL, Tokyo, Japan) at a voltage of 5 kV coupled with an energy dispersive

X-ray detector.[38] For electrochemical characterization, the potential of Zn/Ag printed microcurrent cloth was evaluated by a high-precision voltmeter. The copper clips mounted on the printed area and the unprinted fabrics were used as references with a distance of 1.5 cm, followed by data recording at one data point per second by Keysight/Agilent 34420A.

Preparation of Micelles Without or with Cur Loading

Empty micelles (EMs) and CMs were prepared using a modified self-assembly technique.[52] Generally, Cur was dissolved in solvent (ethanol) at 60°C as the core phase. The shell phase consisting of surfactant or cosurfactant was then added to the core phase with violent stirring at 60°C. A rotavapor (Buchi, R-100, Flawil, Switzerland) was used to remove ethanol at 60°C and rotation speed scale 3. EMs and CMs were obtained, and the resulting samples were stored at 4°C for further evaluation. Tween 20/PEG 400 was used as surfactant/cosurfactant to prepare CMs with large particle sizes (CM-L, Table 1). Kolliphor RH40/Tween 80 was applied to prepare small CMs (CM-S, Table 1).

The average particle size and distributions of EM-L, CM-L, EM-S, and CM-S were determined by dynamic light scattering (DLS, Malvern Nano-ZS, Worcestershire UK).[53] Ten milligrams of each sample were dissolved in 10 mL of water at 25°C. The data showed the mean value of triplicate determinations. The surface morphology of CM-L and CM-S was observed by SEM.[54] Each sample (10 mg) was dissolved in 10 mL of water. A sonicator was then used to help the sample dissolve. After the sample was completely dissolved, 20 µL solution was dropped onto a silicon chip and dried at 40°C in a sample oven. Sample chips were sputter-coated with a thin layer of gold before SEM visualization.

Encapsulation Efficiency and Drug Loading Rate Measurements of Cur in CM-L and CM-S

High-performance liquid chromatography (HPLC) was applied to determine the Cur encapsulation efficiency (EE%) and loading rate (DL%) of CMs with slight modification.[55,56] Briefly, Cur was determined by the Agilent 1260 series (Santa Clara, CA, USA). An Agilent 1260 WR diode array detector is equipped with an Agilent VL quat pump and a Luna 5 µm C18 column (4.6 × 250 mm). An isocratic system of two solvents—50% acetic acid (0.5%) solution (solvent A) and 50% acetonitrile (solvent B)—was used as the mobile phase with a flow rate of 1 mL/min. The injection volume was 20 µL. Detection was performed using a diode array detector with a wavelength of 425 nm. CM-L and CM-S consisting of Cur 20 mg dispersed in water were then collected before and after filtration by using 0.45 µm filters to separate free Cur from CM-L and CM-S. Filtrates were diluted with methanol to dissolve micelles and determined by HPLC. The amount of Cur detected before and after filtration corresponds to the entrapped Cur and the total amount of Cur used, respectively. The encapsulation efficiency and drug loading rate were calculated using equations 1 and 2, respectively.

$$\text{Equation 1}: \ EE\% = \frac{Amount\ of\ entrapped\ curcumin}{Total\ amount\ of\ curcumin\ initial\ used} \times 100\%$$

Table 1 Compositions and Physical Characterization of Micelle Formulations

	Cur (mg)	Surfactant (mg)	Co-Surfactant (mg)	Mean Diameters (nm)/(PDI)	EE% DL%
EM-L	0	Tween 20 (72 mg)	PEG 400 (36 mg)	11.25±0.75 (0.234±0.008)	- -
CM-L	40	Tween 20 (72 mg)	PEG 400 (36 mg)	142.90±1.62 (0.319±0.097)	97.67±1.68 26.47±1.27
EM-S	0	Kolliphor RH40 (140 mg)	Tween 80 (10 mg)	10.27±0.11 (0.110±0.004)	- -
CM-S	10	Kolliphor RH40 (140 mg)	Tween 80 (10 mg)	17.16±0.77 (0.194±0.009)	97.94±0.85 6.13±0.05

Abbreviations: Cur, curcumin; PDI, polydispersity index; EE, encapsulation efficiency; DL, drug loading; EM-L, empty micelle with large particle size; CM-L, curcumin-loaded micelle with large particle size; EM-S, empty micelle with small particle size; CM-S, curcumin-loaded micelle with small particle size.

$$\text{Equation 2}: \quad \text{DL}\% = \frac{\textit{Amount of entrapped curcumin}}{\textit{Total amount of micelle}} \times 100\%$$

Ex vivo Skin Penetration of CMs Formulations with Microcurrent Cloth

The study protocol was approved by the Institutional Animal Care and Use Committee (IACUC) of Chung Hsing University (IACUC number 112002) in accordance with the National Research Council's Guide for the Care and Use of Laboratory Animals. The hair on the back skin of Wistar rats was removed using an electric hair removal knife and hair removal cream, and the remaining subcutaneous tissue was separated. The dermis was gently cleaned with the help of a cotton swab containing isopropyl alcohol to remove residual fat. The prepared rat skin was further washed with phosphate-buffered saline, sealed in aluminum sheets, and stored in a −20°C freezer until use.

Cur and microcurrent cloth were applied to the skin of rat cadavers, covering an area of 3 cm x 3 cm. Groups were divided into Cur, Cur+M (free Cur with microcurrent cloth), CM-S (Cur-loaded micelles with small particle size), CM-S+M (Cur-loaded micelles with small particle size with microcurrent cloth), CM-L (Cur-loaded micelles with large particle size), and CM-L+M (Cur-loaded micelles with large particle size with microcurrent cloth). The amount of Cur used was 20 mg per piece of skin. After two hrs of incubation at room temperature, excess residual preparation containing the formulation was carefully removed from the skin surface. After exposure, skin samples were fixed with 4% paraformaldehyde for 24 hrs. Fixed skin samples were embedded in an optimal cutting temperature compound and frozen overnight in a deep freezer at −80°C. Frozen skin samples were transected into 10 μm thick sections using a Leica CM1520 cryostat (Leica Microsystems, Wetzlar, Germany). After washing with phosphate-buffered saline (PBS), cross-sections of skin samples were taken with a Leica SP5 confocal laser scanning microscope (Leica Microsystems, Wetzlar, Germany).

FTIR and NMR Investigations of CMs Formulations

To investigate the interactions between curcumin and surfactant/cosurfactant, a Fourier transform infrared (FTIR) spectrometer (PerkinElmer, Waltham, MA, USA) equipped with an Attenuated Total Reflectance accessory was used. Spectra were collected over a scan range of 4000–450 cm^{-1} with a scan number of 10 and resolution of 4 cm^{-1} and analyzed using the Origin Pro 8.6 program (Origin Lab Inc., Northampton, MA, USA).[57]

To determine whether the Cur loaded into CMs or not, ^{1}H nuclear magnetic resonance (NMR) analyses were performed using Agilent 400-MHz NMR spectrometer (Agilent, Santa Clara, CA, USA) with 128 scans. Data analysis was performed using Mestrenova NMR software. Samples, Tween 20, PEG 400, Cur, and CM-L were analyzed in DMSO-d_6 and D_2O.[58]

Water Solubility Study of Cur and CM-L

Cur and CM-L (each sample contained 50 mg of Cur) were separately added to 1.5 mL of water. The solution was vortexed for 5 minutes, incubated in a water bath at 37°C overnight and centrifuged at 10,000 rpm for 10 minutes. Supernatants were collected and mixed with methanol (1:1, v/v) to stabilize the curcumin in water. The mixed solution (200 μL) was diluted with methanol. The presence of curcumin was determined by HPLC with slight modification as previous report.[59]

NO Production by CMs Formulations with Microcurrent Cloth

Raw 264.7 cells were seeded into a 24-well plate at 5×10^5 cells/well for 24 hrs and maintained at 37°C under 5% CO_2. The experiment was divided into the control group, LPS (1 μg/mL), general cloth, microcurrent cloth, Cur, Cur +M, CM-L, and CM-L+M. Cells were pretreated with drugs for 6 hrs and then induced with LPS for another 24 hrs. To determine the effect of materials on NO production, the amount of NO in the supernatant was detected using Griess reagent. The absorbance at 540 nm was detected by a microplate reader. The NO content was calculated from a nitrite standard curve.

Enzyme-Linked Immunosorbent Assay (ELISA)

Raw 264.7 cells (5 x 10^5 cells/well) were seeded in 96-well plates and left to adhere overnight. Cells were pretreated with Cur and microcurrent for six hrs and then stimulated with LPS (1 μg/mL) for 12 hrs. The cytokines (IL-6 and IL-10) in the supernatant were measured using an ELISA kit (Invitrogen) according to the manufacturer's instructions.

Transdermal Performance of Cur and CM-L with Microcurrent Cloth

The in vitro transdermal performance of Cur and CM-L was evaluated by a Logan DHC-6T(New Jersey, USA) transdermal system with slight modification.[60] The transdermal system was composed of donor and receptor cells with capacities of approximately 3 mL and 13 mL, respectively. The Strat-M membrane was applied for transdermal performance evaluation. It was fixed securely between the donor and the receptor cell with an effective diffusion area of approximately 1.77 cm^2. Cur and CM-L samples (each sample contained 10 mg of Cur) were dispersed in phosphate-buffered saline pH 7.4 (PBS) and applied to the donor cells. The receptor cell was filled with medium (containing PBS pH 7.4 with 1% Tween 80), stirred with a mini magnetic stirring bar, and maintained at 32°C. Microcurrent clothes were placed on the Strat-M membrane to evaluate the transdermal efficacy of Cur. Samples were collected from receptor cells at predetermined time points. Fresh medium was then immediately added to each receptor cell. Samples were diluted with methanol and stored in a refrigerator at 4°C prior to HPLC analysis.

Surgical Procedures for Full-Thickness Wounds and Administration of CMs Formulations with Microcurrent Cloth

The animal test was approved by the Institutional Animal Care and Use Committee (IACUC) of National Chung Hsing University (IACUC number 112–029). All animal experiments were performed according to guidelines of the Chung Hsing University Institutional Animal Care and Use Committee.

Mice were anesthetized, and the hair on their dorsal area was removed using an electric shaver and depilatory cream a day before the surgery. Wounds were established and modified based on the methods used in a previous report.[61] To summarize, the mice were anesthetized with isoflurane (2%) in oxygen via a facemask. One 8-mm full-thickness circular wound was then created on the backs of the mice using sharp surgical instruments and forceps. The injuries were covered with a Tegaderm sterile dressing (3 M Healthcare, St. Paul, MN, USA) to prevent eschar formation on the wounds and stop the mice from scratching.

After surgically creating full-thickness circular wounds, the mice were randomly assigned to one of the following groups: (a) the control group, treated with PBS; (b) the Cur group; (c) the Cur+M group; (d) CM-L group; and (e) CM-L +M group. Each administered dose (containing 0.375 mg of Cur) was applied topically every two days and covered with a new microcurrent and 3M sterile dressing (3M Healthcare, St. Paul, MN, USA).

Physical Parameters and Histopathology Evaluation

Photos were taken every two days for eight days during the wound-healing process. The wound areas were calculated using equation 3 in pixels with ImageJ 1.53 software (Nation Institutes of Health, USA). The wound sizes were expressed as a percentage of the initial wound area.

$$\text{Equation 3 : Wound closure \%} = \left(1 - \frac{wound\ area\ onday\ n}{wound\ area\ onday\ 0}\right) \times 100\%$$

The wound specimens were fixed with 10% formalin. After routine processing and embedding in paraffin, 4-μm-thick sections were cut and stained with hematoxylin, eosin, and Masson's trichrome for collagen. The slides were scanned with a slide scanner (Philips, Amsterdam, Netherlands).

Statistical Analysis

All experimental data from the studies was analyzed statistically. The results are expressed as the mean ± standard deviation (SD). Statistical differences (*$P < 0.05$) were calculated using one-way ANOVA followed by a Tukey post hoc test for multiple comparisons with SPSS, version 24 (IBM).

Results and Discussion

Characterization of Microcurrent Cloth with Printed Zn/Ag Electroceutical Fabric

SEM analysis revealed the deposition of Ag and Zn particles on the fibers of the cellulose fabric used in the general cloth. SEM imaging of the general cloth showed a different weaving pattern than the Zn/Ag printed microcurrent cloth shown in Figure 2A. The SEM images of the Zn/Ag printed pattern vividly demonstrated that the metallic particles formed a layer over the underlying silk fibers, as shown in Figure 2B. Further analysis using energy-dispersive X-ray spectroscopy (EDX) confirmed the presence of Ag and Zn on the microcurrent cloth, while the general cloth lacked these elements, as shown in Figure 2C and D.

The Zn/Ag-printed microcurrent cloth used for testing the electroceutical properties consisted of cellulose fabric with printed-designed regions. These regions alternated between different inks with different compositions. To evaluate the electroceutical properties of microcurrent cloth, the surface contact potential was measured within a two-dimensional area and the measurements were compared to the potential of the general cloth, which served as a reference. The proximity of Ag and Zn on the cellulose fabric created some redox electrochemical reactions, enabling electrochemical reactions when the fabric comes into contact with wet environments containing ions, such as body fluids. Here, two aqueous media were tested: nonionic water and the ionic solution PBS. The microcurrent cloths showed detectable electric potentials only when moist. The experimental setup was at first dry and then moistened by water or PBS after 5 seconds. The cloth was totally moistened at 25 seconds, when a significant change in potential was recorded, as shown in Figure 3. The average potential of the microcurrent cloth was measured as +101.3 mV in water, while the average potential was +214.6 mV in PBS. These results indicate that the Zn/Ag-printed patterns on the fabric generated electrical potential.

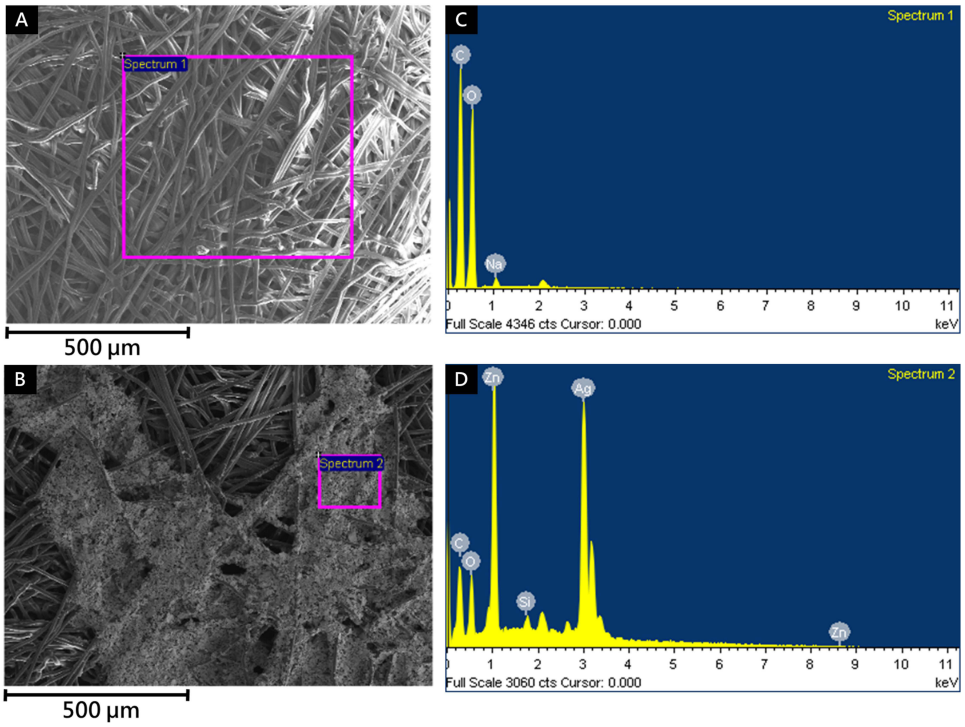

Figure 2 SEM images and EDX analysis of general cloth and microcurrent cloth. SEM image of (**A**) general cloth and (**B**) Zn/Ag printed microcurrent cloth. EDX analysis of (**C**) general cloth and (**D**) Zn/Ag printed microcurrent cloth. Scale bar: 500 µm.
Abbreviations: SEM, scanning electron microscopy; EDX, energy-dispersive X-ray spectroscopy.

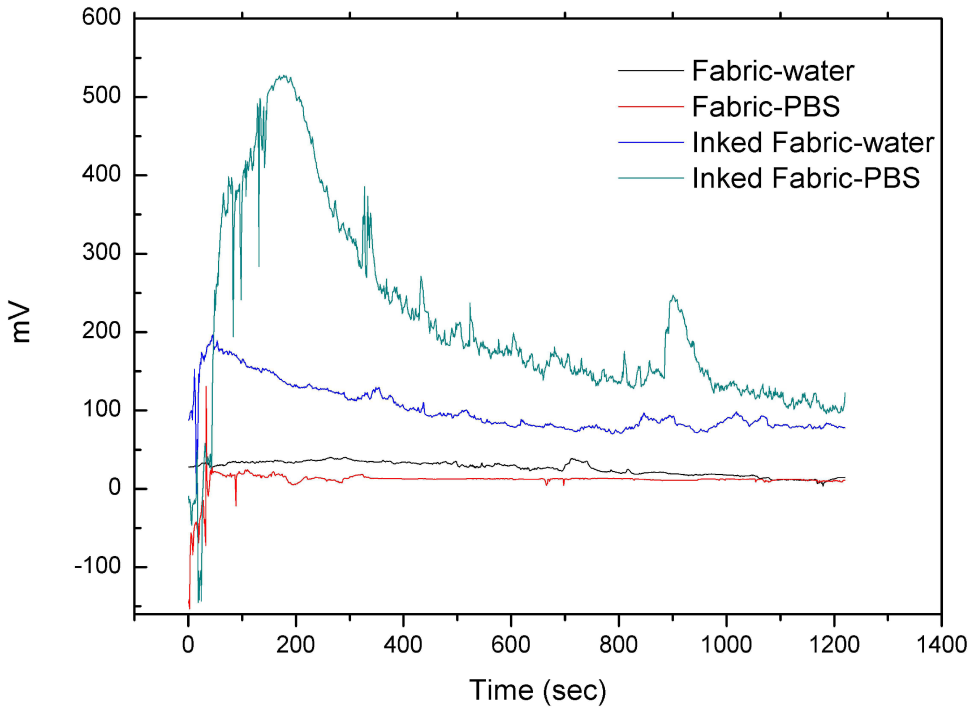

Figure 3 The electroceutical properties of Zn/Ag printed microcurrent cloth. Black line: the potential measurement of the general cloth in water. Red line: the potential measurement of the general cloth in PBS. Blue line: the potential measurement of the microcurrent cloth in water. Green line: the potential measurement of the microcurrent cloth in PBS.

Preparation and Characterization of CMs Formulations

Self-assembled Cur-loaded micelle formulations were successfully prepared by using various surfactants and cosurfactants in a one-pot process. Similar results were obtained in a previous study in which Kolliphor RH40 and Tween 80 were used as surfactants and cosurfactants to successfully prepare small micelle formulations.[52] The compositions and particle size analysis of empty micelles with small particle sizes (EM-S) and CM-S performed by the DLS method are summarized in Table 1. As shown in Figure 4A2 and Table 1, EM-S and CM-S showed small average diameters of 10.27±0.11 nm and 17.16±0.77 nm along with narrow polydispersity indices (PDIs) of 0.110±0.004 and 0.194±0.009, respectively.

Tween 20 and polyethylene glycol (PEG) have been applied in Cur encapsulations to improve the encapsulation efficiency, stability, and solubility of Cur.[62–64] Therefore, the optimized compositions of Tween 20 and PEG 400 were also used for the preparation of CM-L (as shown in Table 1). Empty micelles with large particle sizes (EM-L) and CM-L were prepared with particle sizes on the order of 11.25±0.75 and 142.9±1.62 nm along with PDIs of 0.234±0.008 and 0.319±0.097, respectively (Figure 4A1 and Table 1).

Since Cur belongs to class IV in the Biopharmaceutical Classification System (BCS) indicating poor solubility in aqueous solutions and poor intestinal permeability of curcumin.[65] Unformulated Cur in aqueous solution can be easily separated with a 0.45 μm filter. Therefore, EE% was also measured to evaluate the encapsulated efficiency of Cur. Both CMs formulations exhibited excellent EE%: 97.67% for CM-L and 97.94% for CM-S, as shown in Table 1. Recent research has indicated that most nanoparticle drug delivery systems have relatively low drug loading (less than 10%), and the development of delivery systems to increase the drug loading rate remains a challenge.[66] Remarkably, the DL% was increased from 6.13% for CM-S to 26.47% for CM-L, as shown in Table 1, showing improved efficiency for bioactivity applications.

The surface morphology of the CMs formulation was observed using SEM. Smooth surface morphology with a particle size of approximately 100 nm of CM-L was observed from the SEM image (Figure 4B1 and C1). From Figure 4B2, it can be noted that the shape of the nanoparticles was irregularly circular with an average particle size of approximately 100 nm. These nanoparticles represented the self-aggregated state consisting of CM-S and an average particle size of approximately 30 nm (Figure 4C2).

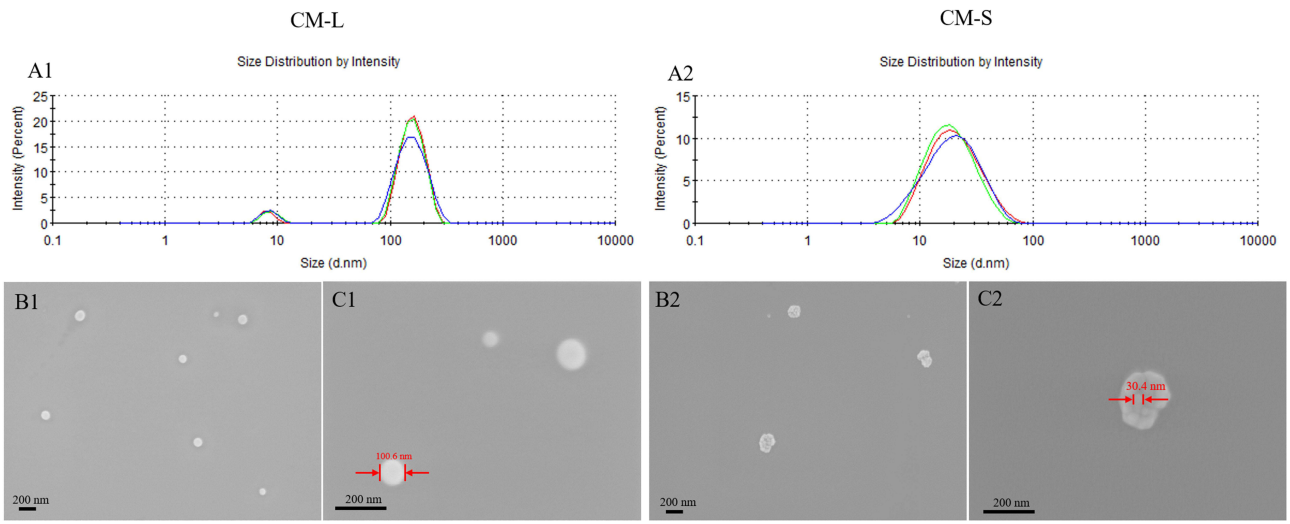

Figure 4 Size distribution and morphology of curcumin-loaded micelle formulations with large particle size (1) and small particle size (2). (**A**) Particle size distribution was determined by dissolving 10 mg samples in 10 mL double distilled water (ddH_2O) and analysis by DLS at 25°C. (**B**) SEM images were acquired by dissolving 10 mg samples in 10 mL of ddH_2O and then dropping 20 μL of the sample solution onto a silicon chip and drying at 40°C in a sample oven. Finally, the sample chip was sputter-coated with a thin layer of gold for SEM visualization. (**C**) SEM image with a large-scale view and calculated particle size. Scale bar: 200 nm.
Abbreviations: CM-L, curcumin-loaded micelle with large particle size; CM-S, curcumin-loaded micelle with small particle size; DLS, dynamic light scattering; SEM, scanning electron microscopy.

Ex vivo Skin Penetration of CMs Formulations with Microcurrent Cloth

Ex vivo permeation experiments showed the permeation amount of curcumin-loaded micelle formulations and the penetration effect of microcurrent cloth. As shown in Figure 5, native Cur barely penetrated the skin, while CM-S and CM-L exhibited excellent skin penetration capacities. It has been reported that the hair follicle tunnel is one of the penetration paths for nanoparticle transdermal delivery and that the penetration amount and depth depend on the particle size.[40] Knorr et al have also pointed out that larger nanoparticles are deposited in the hair follicle duct, while smaller particles with a size of 40 nm can penetrate the skin barrier and transport compounds to specific cell populations.[41] However, a variety of enhancement strategies have been developed to overcome the natural barrier function of skin to

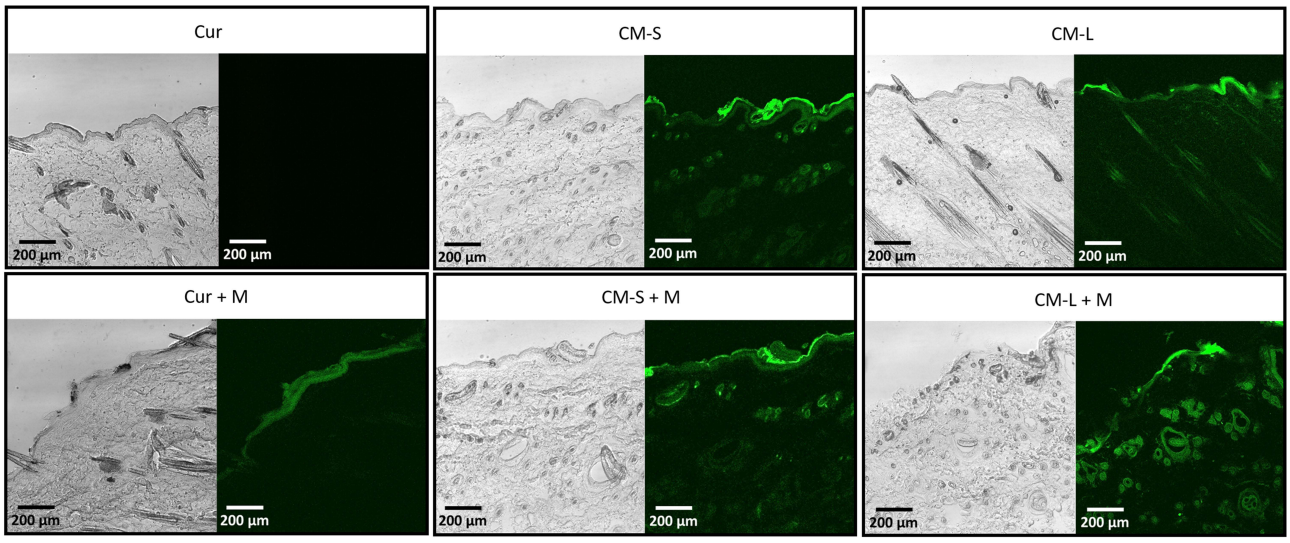

Figure 5 CLSM images of the rat skin penetration of curcumin-loaded micelle formulations with different particle sizes without or with of microcurrent cloth. Right side of each picture indicates the fluorescence image of curcumin, and left side pictures are bright view images. Scale bar: 200 μm.
Abbreviations: CLSM, confocal laser scanning microscopy; Cur, free curcumin; Cur+M, free curcumin with microcurrent cloth; CM-S, curcumin-loaded micelle with small particle size; CM-S+M, curcumin-loaded micelle with small particle size with microcurrent cloth; CM-L, curcumin-loaded micelle with large particle size; CM-L+M, curcumin-loaded micelle with large particle size with microcurrent cloth.

facilitate transdermal penetration and absorption of active compounds. It has been demonstrated that electrostatic potential and microcurrent can reduce the barrier function of skin and increase the penetration of drugs by relaxing lipid molecule accumulation in the stratum corneum and forming transient permeability pores.[67,68] To address these findings, microcurrent clothes were applied to evaluate the skin penetration ability of CMs. As shown in Figure 5, both the CM-S+M and CM-L+M groups exhibited an increased transdermal amount of Cur. Because of the excellent transdermal ability of the small average particle size of CM-S, microcurrents did not significantly improve the skin penetration amount. Similar to the literature results, large-sized nanoparticles such as CM-L can accumulate in hair follicles.[41] Interestingly, microcurrent-assisted treatment not only increases the accumulation of CMs in hair follicles, but also enhances its therapeutic effect by promoting the escape of CM-L from the hair follicle barrier. CM-L and microcurrent cloth were mainly applied for further evaluation.

FTIR and NMR Investigations of CM-L Formulations

FTIR spectrum was used to further identify the encapsulation property of CM-L. Figure 6 illustrates the FTIR spectrum of Tween 20, PEG 400, Cur, and CM-L. In the spectrum of surfactant Tween 20 and PEG 400 (shown in Figures 6A and B), the peak around 3676 cm^{-1} is attributed to hydrogen-bonded O-H stretching vibrations. The peaks at 2988 cm^{-1}, 2973 cm^{-1}, and 2902 cm^{-1} are due to the asymmetric and symmetric stretching vibrations. The peak at 1735 cm^{-1} is due to the carbonyl group. The other characteristic peaks are presented at 1394 cm^{-1}, 1250 cm^{-1}, 1066 cm^{-1}, and 892 cm^{-1}. In Figure 6C, which represents the FTIR spectrum of Cur, the stretching of the functional group OH is indicated at 3513 cm^{-1}. The peak at 1627 cm^{-1} and 1509 cm^{-1} indicated the function groups C=O and C=C, respectively. Other characteristic peaks of Cur include 1280 cm^{-1} and 1154 cm^{-1}. Most of the characteristic peaks of Tween, PEG, and Cur were present in the FTIR spectrum of CM-L, as shown in Figure 6D. The most striking feature of the micelle FTIR

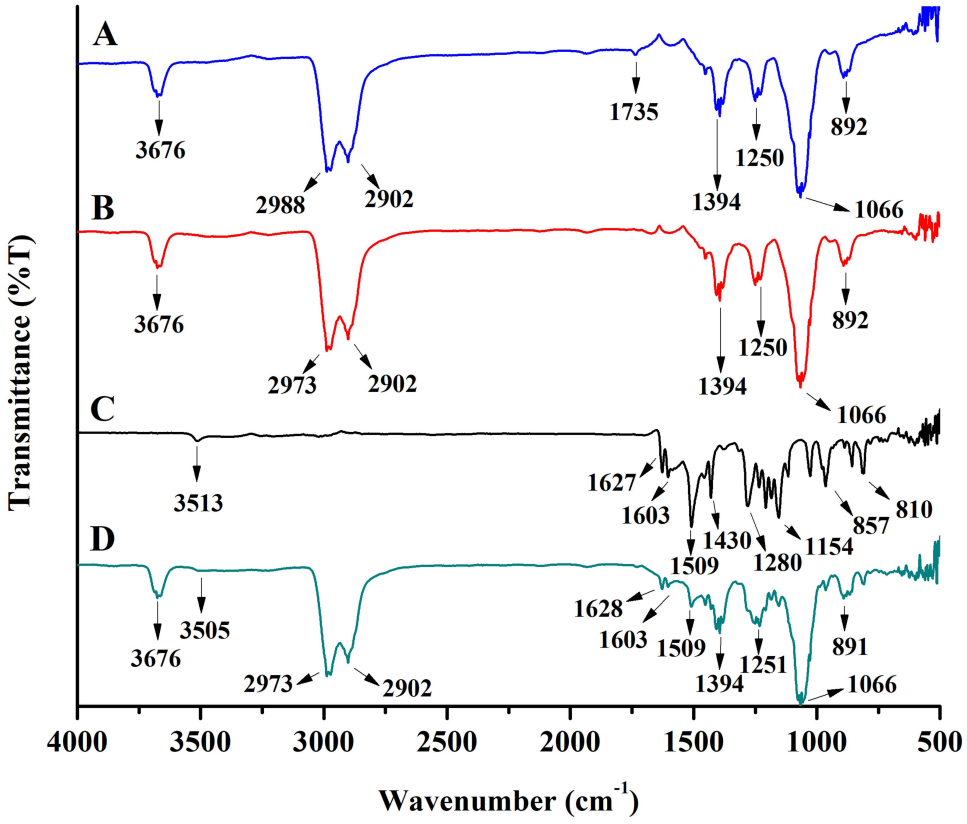

Figure 6 FTIR spectrum of Tween 20 (**A**), PEG 400 (**B**), Cur (**C**), and CM-L (**D**).
Abbreviations: FTIR, Fourier transform infrared; PEG, polyethylene glycol; Cur, curcumin; CM-L, curcumin loaded micelle with large particle size.

spectrum is the band shift of the O-H stretching from 3513 cm^{-1} to 3505 cm^{-1} for encapsulated Cur in micelle formulation compared to native Cur.

^{1}H NMR is a powerful tool to study an encapsulated micelle. Tween 20 and PEG 400 were dissolved in DMSO-d_6 and spectrums were obtained as shown in Figures 7A and B, respectively. Cur was dissolved in DMSO-d_6. The specific peak of the aromatic ring was obtained between 6.50 and 7.60 ppm, as shown in Figure 7C. Notably, CM-L dissolved in DMSO-d_6 and D_2O presented different spectra, as shown in Figures 7D and E. In Figure 7D, the characteristic peak of composition can be seen, especially the characteristic peak of Cur. However, when CM-L is dissolved in D_2O, as shown in Figure 7E, the characteristic signal of Cur at 6.5–7.6 is weak. It is speculated that in a D_2O environment, Cur is encapsulated in self-assembled micelles, thus blocking the characteristic signal of Cur. Similar results can also be seen in previously published hyaluronic acid nanoemulsions.[69]

Water Solubility Study of CM-L

The solubility of CM-L (Cur 50 mg/1.5 mL) in water was compared with that of native Cur, and the solutions were collected and analyzed by HPLC to confirm the presence and exact concentrations of Cur in water. The results indicated that the Cur solubility of Cur and CM-L was 8.68 μg/mL and 2143.67 μg/mL, respectively (Figure S1). The solubility of native Cur was similar to the result published from Maiti's research.[70] Based on these results, the water solubility of Cur was effectively enhanced by approximately 250-fold, which possibly enhanced the bioavailability and wide use of Cur in pharmaceutical applications.

Evaluation of the Ability of Cur and Microcurrent to Inhibit the Production of NO

NO can be used as an indicator of the presence of inflammation.[71] The Griess reaction test was used to measure the level of NO by comparing its absorbance with prepared standards to quantify the nitrite ions contained in the sample. As shown in Figure 8, LPS stimulated macrophages to induce inflammation with an increase in NO production around 15 μM. The general cloth exhibited a low contribution to suppressing NO production. In contrast, the microcurrent cloth significantly reduced NO production after LPS stimulation. Cur has been considered an anti-inflammatory agent that inhibits NO production.[72] Here, both Cur and CM-L revealed effective inhibition abilities on NO production. Since the

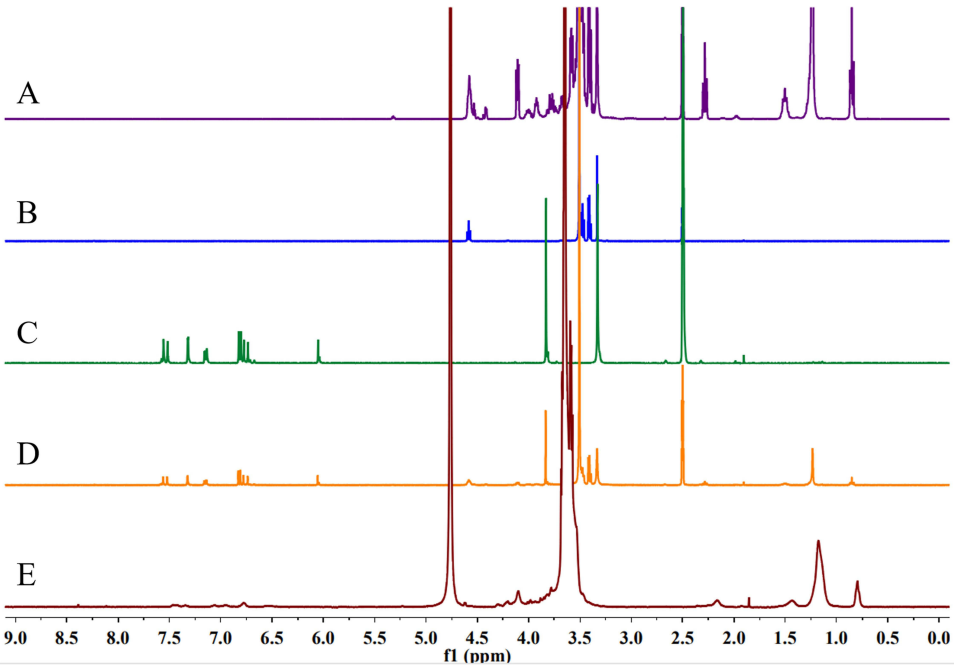

Figure 7 ^{1}H NMR spectrum of Tween 20 (**A**), PEG 400 (**B**), Cur (**C**), CM-L dissolved in DMSO-d_6 (**D**), and CM-L dissolved in D_2O (**E**).
Abbreviations: NMR, nuclear magnetic resonance; PEG, polyethylene glycol; Cur, curcumin; CM-L, curcumin loaded micelle with large particle size.

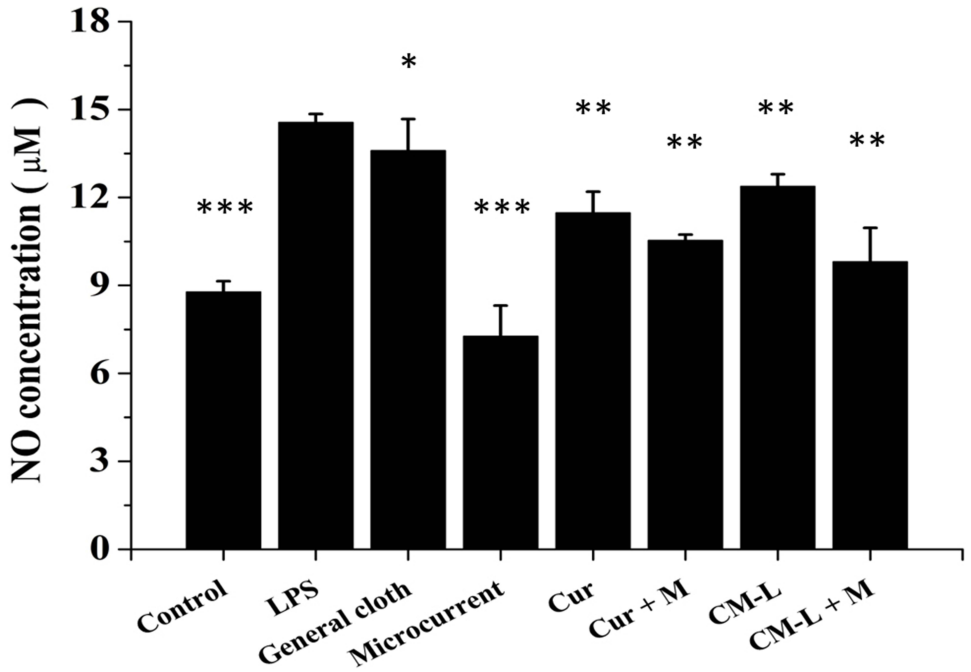

Figure 8 NO production effect by curcumin-loaded micelle formulations and microcurrent cloth. Raw 264.7 macrophages were exposed to LPS (1 μg/mL) for 24 h and then treated under different conditions. After 24 h, the nitrite concentration in the supernatant reflecting NO production was measured using the Griess reagent. Data are expressed as the mean ± SD (n = 3). *p < 0.05, **p < 0.01, ***p < 0.001 compared with LPS by *t*-test).

Abbreviations: NO, Nitric oxide; LPS, lipopolysaccharide; Cur, free form curcumin; Cur+M, free form curcumin with microcurrent cloth; CM-L, curcumin loaded micelle with large particle size; CM-L+M, curcumin loaded micelle with large particle size with microcurrent cloth. SD, standard deviation.

microcurrent cloth showed an excellent ability to reduce NO production, the combined treatment groups (Cur+M and CM-L+M) presented a more significant ability to inhibit NO production compared to the Cur or CM-L groups. Korelo et al also reported that lesions treated with the microcurrent group showed activity in inhibiting NO production.[73] It is speculated that the redox reaction of the Zn/Ag electrode oxidizes NO to NO_2, and NO_2 is converted into nitric acid when dissolved in water. The Griess reagent used in NO detection cannot react with NO, resulting in an underestimate of the production of NO. Therefore, cytokines were used to verify the inflammatory capacity.

Effect of Topical Applications of Different Treatments on the Levels of IL-6 and IL-10

It has been reported that macrophages secrete abundant proinflammatory proteins during inflammation, which intensifies inflammation.[74] As shown in Figure 9A, LPS treatment enhanced the expression of IL-6, which was reduced by treatment with Cur and CM-L. In contrast, treatment with the microcurrent cloth increased IL-6 production, which also influenced and increased IL-6 production in the two combined treatment groups (Cur+M and CM-L+M). IL-10 is considered an anti-inflammatory cytokine that improves the transition of injured tissue from the inflammatory phase to the proliferative phase.[75] In this experiment, increased expression of IL-10 was not observed in most groups, as shown in Figure 9B. In contrast, a significant improvement in IL-10 expression was observed in all microcurrent cloth treatment groups, microcurrent groups, Cur+M, and CM-L+M.

Generally, IL-6 and IL-10 are considered proinflammatory and anti-inflammatory cytokines, respectively. Interestingly, the expression levels of IL-6 and IL-10 were both enhanced in the microcurrent cloth treatment group. It has been demonstrated that IL-6 exhibits multiple functions in inflammatory and reparative processes, promoting Th2 and Th17 differentiation in CD4+ T cells, inhibiting TGF-β-dependent differentiation of T regulatory cells, eliciting endocrine signals that result in platelet production within the bone marrow critical for hemostasis, and initiating profibrotic fibroblast/keratinocyte interactions.[76] The mechanism of microcurrent-associated IL-6 secretion are necessary to be investigated in the near future.

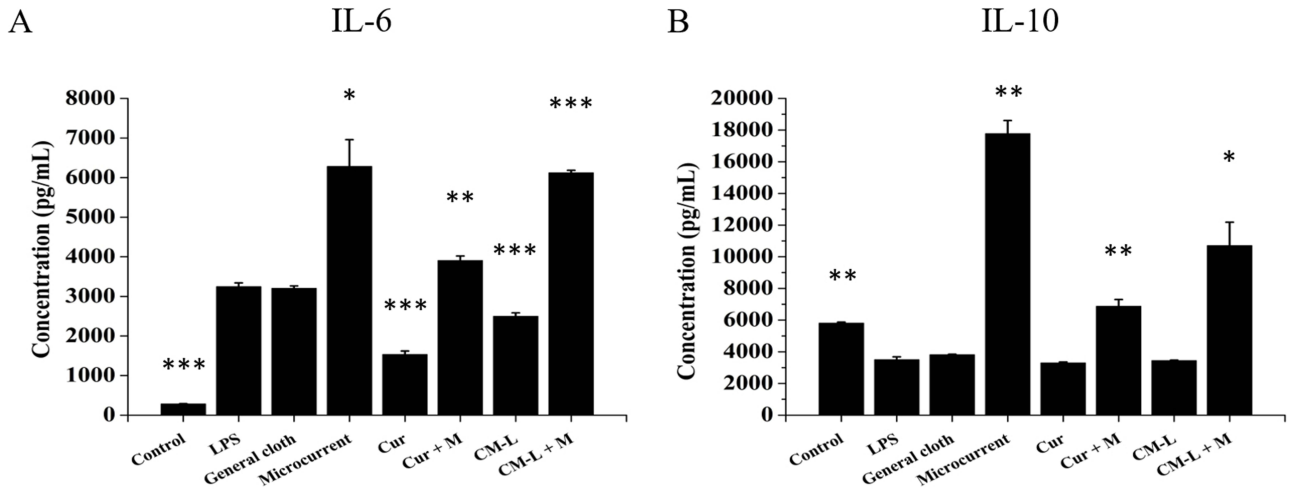

Figure 9 Cytokine, IL-6 (**A**) and IL-10 (**B**) generation effect by curcumin-loaded micelle formulations and microcurrent cloth. Raw 264.7 macrophages were exposed to LPS (1 μg/mL) for 24 h and then treated under different conditions. After 24 h, cell-free culture medium was collected and analyzed using IL-6 and IL-10 ELISA kits. Data are the mean ± SD from 3 independent experiments*$p < 0.05$, **$p < 0.01$, ***$p < 0.001$ compared with LPS by *t* test).

Abbreviations: IL-6, interleukin-6; IL-10, interleukin-10; LPS, lipopolysaccharide; Cur, free curcumin; Cur+M, free curcumin with microcurrent cloth; CM-L, curcumin-loaded micelles with a large particle size; CM-L+M, curcumin-loaded micelles with a large particle size with microcurrent cloth; SD, standard deviation.

Transdermal Performance of Cur and CM-L with Microcurrent Cloth

The in vitro transdermal performance of Cur and CM-L was evaluated by using a Strat-M membrane. Takashi et al have suggested that Strat-M could replace excised human or rat skin in conducting transdermal studies with nanoparticles.[77] Solvents or solubilizers are often employed in the receptor cell to ensure sink conditions when dealing with hydrophobic components.[78] However, some studies have reported that solvents such as ethanol may disrupt skin integrity.[79] Therefore, in this study, 1% Tween 80 was used in the receptor medium to increase the solubility of Cur and maintain sink conditions.[80]

Figure 10 demonstrates the enhanced transdermal performance of CM-L with microcurrent cloth treatment. The 24-hr permeation profile of curcumin is shown in Figure 10A. The cumulative amount of Cur permeated for 24 hr in the Cur and Cur+M groups was 16.66 ± 2.82 and 24.33 ± 2.43 μg/cm^2, respectively. Microcurrent cloth slightly enhanced 1.46-fold of permeability of Cur. Meanwhile, the permeation of Cur from CM-L (155.18 ±19.86 μg/cm^2) was significantly increased 9.31-fold compared with that of unformulated Cur. Exhilaratingly, microcurrent assisted treatment, CM-L+M, significantly increased skin penetration of curcumin in 20.01-fold (3105.43 ± 23.28 μg/cm^2) than that of CM-L group. The results indicated microcurrent not only facilitates the transdermal ability of Cur, but also improves the skin permeability of large particle size such as CM-L. The flux values at 24 hr, as shown in Figure 10B, were calculated as 0.69±0.13, 6.45±1.19, 1.01±0.11, and 124.42±21.82 μg/cm^2, represented as Cur, CM-L, Cur+M, and CM-L+M, respectively. After a 24-hr transdermal experiment, Strat-M was collected, and the content of Cur on the membrane was further quantified. Formulated Cur (CM-L) increased the content of Cur on the Strat-M membrane, especially in the effective diffusion area, as shown by the red circular dotted line in Figure 10C. The content and distribution of Cur on the Strat-M membrane were also consistent with the pattern on the microcurrent cloth. Figure 10D shows that CM-L, Cur +M, and CM-L+M increased the content of Cur on the Strat-M membrane 2.83, 2.08, and 5.52 fold (respectively) compared with native Cur.

We further analyzed the flux values to investigate the kinetic transdermal penetration capacity of Cur. In according to the results in Figure 10A, the phenomena of penetration can be obviously divided into two stages: a rapid penetration stage (0–4 hrs) and a sustained release stage (6–24 hrs). In the rapid penetration stage, CM-L+M group showed the excellent flux value in an average of 610.58 μg/hr/cm^2 whereas the flux value of CM-L group was only 2.74 μg/hr/cm^2. The Cur and Cur+M groups also showed relatively low fluxes of 0.00 μg/hr/cm^2 and 0.71 μg/hr/cm^2, respectively. In the sustained release stage, the Cur and Cur+M groups still exhibited relatively low fluxes of 0.63 μg/hr/cm^2 and 1.49 μg/hr/cm^2, respectively. The flux of the CM-L+M group dropped from 610.58 μg/hr/cm^2 to 315.48 μg/hr/cm^2, representing

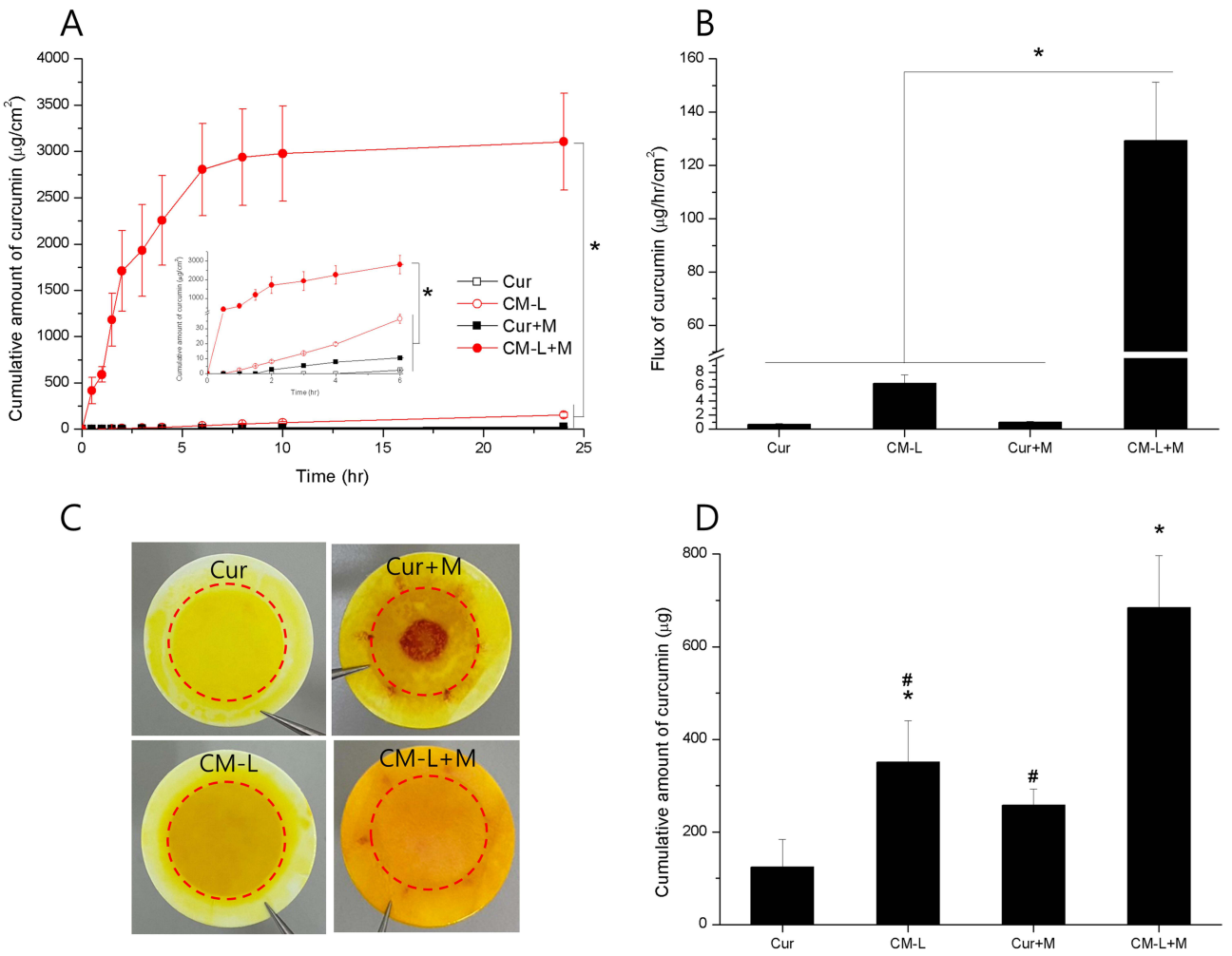

Figure 10 Transdermal performance effect of curcumin-loaded micelle formulations and microcurrent cloth. (**A**) Permeation of curcumin through the Strat-M membrane in different formulations. Black empty square: Cur, black solid square: Cur+M, red empty circle: CM-L, red solid circle: CM-L+M. The small picture in the picture shows the transdermal performance from 0 to 6 hr. Statistically significant differences are indicated by *($p < 0.05$). (**B**) The flux value of curcumin in different formulations at 24 hr. Statistically significant differences are indicated by *($p < 0.05$). (**C**) The donor side Strat-M image of different curcumin formulations after 24 hr transdermal evaluation. The red circular dotted line indicates the effective diffusion area. (**D**) The cumulative amount of curcumin on the Strat-M membrane after 24 hr transdermal evaluation. Data are expressed as the mean ± SD (n = 3). Statistically significant differences are indicated by *($p < 0.05$) compared with cur and #($p < 0.05$) compared with CM-L+M.
Abbreviations: Cur, free form curcumin; CM-L, curcumin-loaded micelle with large particle size; Cur+M, free form curcumin with microcurrent cloth; CM-L+M, curcumin-loaded micelle with large particle size with microcurrent cloth; SD, standard deviation.

a starting trend of slow release. However, this flux value is still much higher than 6.70 μg/hr/cm^2 of CM-L, indicating that the potential of enhanced skin permeability of CMs using microcurrent-assisted strategy.

Therapeutic Effects of Cur with or Without Microcurrent

Clinical and preclinical studies have consistently shown that the main causes of wound nonhealing are oxidative damage, infection, and inflammation.[81] Traditional herbal medicines with anti-infective, anti-inflammatory, and antioxidant properties (such as Cur) have been well studied and applied in wound healing.[27] The wound-healing process was observed every two days, and wound images were captured as shown in Figure 11. On day 2, both the CM-L and CM-L+M groups showed higher wound-closure rates (50.92% and 55.96%, respectively) than the control group (23.48%), Cur group (34.10%), and Cur+M group (32.77%).

Significant clinical evidence has shown that exogenous microcurrent can accelerate the repair process of skin wounds at the physiological level.[82,83] The combined application of the CM-L+M group exhibited a better wound-closure rate (77.94%) than the control group (49.27%) on day 4. Meanwhile, the wound-closure rates on day 4 of the Cur, Cur+M, and CM-L groups were

61.59%, 63.81%, and 64.73%, respectively. On day 8, the wounds of all five groups appeared dry and not infected, with a wound closure rate greater than 90%. As shown in Figure 11B, formulated Cur accelerated short-term (within 2 days) wound healing due to its rapid permeation properties. For a long-term treatment evaluation, Cur, Cur+M, and CM-L treatments exhibited similar wound-closure abilities. Overall, the CM-L+M group showed higher wound healing than the other four groups during the observation period.

Bacterial infection affects the physiological pattern of wound repair, making it difficult for wounds to heal. Therefore, many strategies for fighting bacteria have been developed to improve the treatment of infected wounds, reduce healing time, and reduce health risks (including side effects and toxicity). Nanocarriers and hydrogels were developed for the delivery of antibacterial agents.[23,31,84] However, drug resistance issues and the skin barrier still limit the effectiveness of nanocarriers in wound repair. Therefore, photothermal therapy and photodynamic therapy are used to disrupt the skin barrier and resolve drug resistance. For example, silver nanoparticles and copper nanoparticles are used as antimicrobial agents for photothermal therapy (PTT).[85] Some research revealed that Cur combined with photodynamic therapy (PDT) as an antibacterial agent for wound repair.[86] However, both PDT and PTT require additional equipment and energy to promote the absorption of Cur and exert its therapeutic effects. In this research. In this study, microcurrent cloth was used to eliminate the skin barrier and increase CMs permeability without requiring additional equipment and energy. Microcurrent-assist combined treatment avoids the secondary damage and side effects of PTT and PDT on the wound surface and maintains the feasibility of future combined treatment with phototherapy.

The Effect of Different Treatment Modalities Applied Topically on Histopathological Changes in Healing Tissue

Hematoxylin and eosin (H&E) staining was used to assess the healing status of the wound tissue. At the end of day 8, all groups exhibited complete regeneration of most of the epidermis, as illustrated in Figure 12A. Additionally, the length of the dermal gap was used as an indicator to evaluate the effectiveness of different treatment options.[87] Both the Cur+M

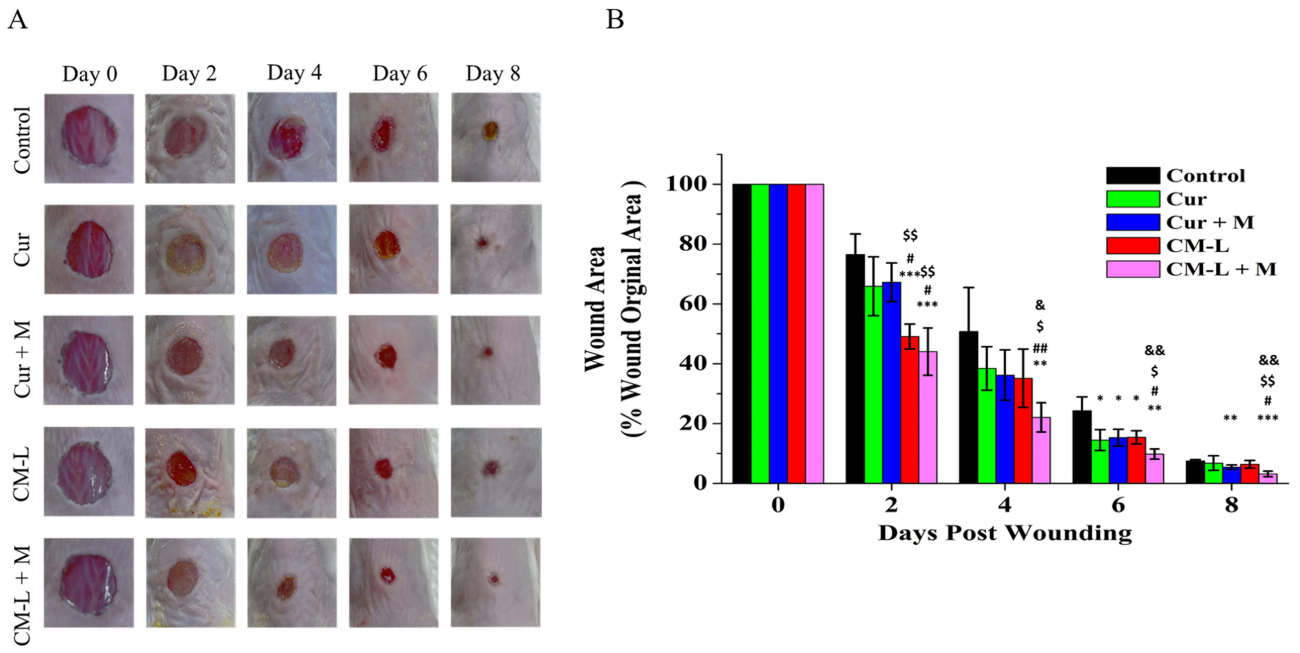

Figure 11 In vivo wound healing effect of curcumin-loaded micelle formulations and microcurrent cloth. (**A**) Effect of the curcumin and loaded micelle formulations with and without microcurrent on wound healing from day 0 to day 8. Images were taken every 2 days during treatment. (**B**) Area percentage of mouse wound healing. (mean ± SD; *: P < 0.05, **: P< 0.01, ***: P < 0.001 compared with the control; #: P <0.05, ##: P<0.01 compared with Cur; $ < 0.05, $$< 0.01 compared with Cur + M; &: P < 0.05, && <0.01 compared with CM-L.

Abbreviations: Cur, free curcumin; Cur+M, free curcumin with microcurrent cloth; CM-L, curcumin-loaded micelles with large particle sizes; CM-L+M, curcumin-loaded micelles with large particle sizes with microcurrent cloth; SD, standard deviation.

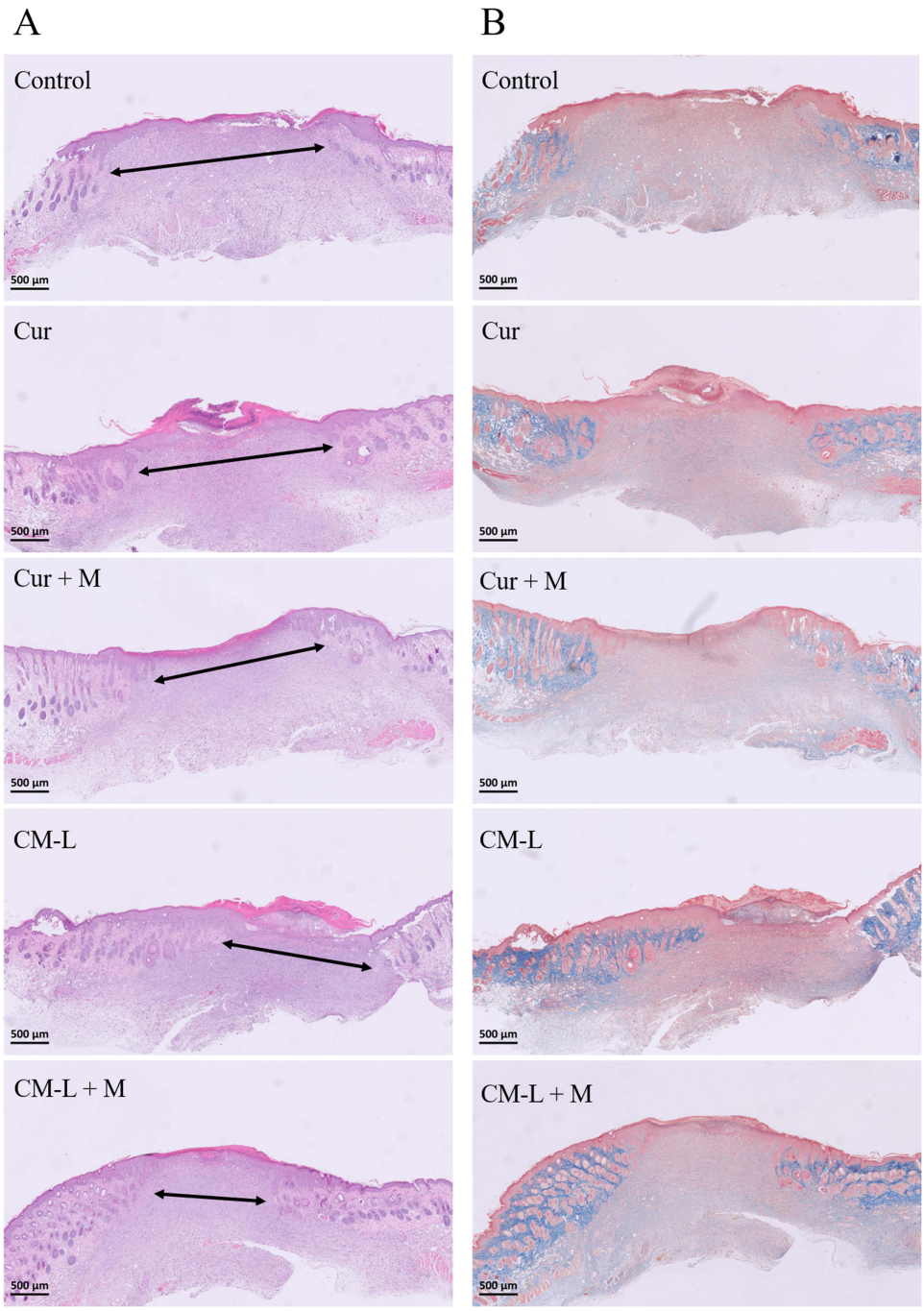

Figure 12 Histopathological results of wound sites on day 8 treated with curcumin-loaded micelle formulations and microcurrent cloth. The length of the arrow indicates the length of the dermal gap. (**A**) H&E staining. (**B**) Masson's trichrome staining. (magnifications 2x, bar = 500 μm).
Abbreviations: H&E, hematoxylin and eosin; Cur, free form curcumin; Cur+M, free form curcumin with microcurrent cloth; CM-L, curcumin-loaded micelle with large particle size; CM-L+M, curcumin-loaded micelle with large particle size with microcurrent cloth.

and CM-L treatment groups showed a slight narrowing of the dermal gap when compared to the control and Cur groups. Notably, the CM-L+M group demonstrated significant repair results in the dermis, substantially reducing the gap distance compared to all other groups. Furthermore, Masson's trichrome staining provided additional evidence supporting the healing status of the wound tissue (Figure 12B). Collagen appeared blue, nuclei dark brown, muscle tissue red, and cytoplasm pink in the staining.[88,89] Consistent with the H&E staining results, the Cur+M and CM-L treatment groups displayed a larger collagen infiltration area in the dermis than the control and Cur groups. However, the CM-L+M group

exhibited a significantly greater infiltration area of collagen in the dermis than any other group. Overall, these findings demonstrated the positive impact of the Cur+M and CM-L treatments on wound healing, with the CM-L+M group showing particularly promising results in promoting collagen regeneration in the dermal tissue.

The primary distinction between the CM-L and Cur groups was determined in the nanoencapsulation, which resulted in enhanced drug stability and improved solubility in water.[90] Nevertheless, upon comparing the CM-L group with both the Cur and Cur+M groups, no clear difference in wound healing was observed. Remarkably, the CM-L+M group (a combination of CM-L with microcurrent cloth) exhibited a significant difference compared to the other groups. This phenomenon can be attributed to the synergistic effect of microcurrent stimulation on wound repair, combined with the carrier's enhanced ability to penetrate or release the drug.[91–93]

Effect of Topical Applications of Different Treatments on Collagen Synthesis in the Healing Tissues

Previous research has indicated that the low density of regenerated collagen in the dermis can lead to reduced elasticity in the regenerated tissue. Therefore, achieving a comparable density of collagen regeneration is essential to ensuring biophysical continuity between the original and new skin tissue.[67] In this context, the density of regenerated collagen in the dermis was measured using Masson's trichrome (M-T) stained images, determined by the intensity of the staining signal in equal areas (as depicted in Figure 13). The collagen intensity of the regenerated tissue was approximately 1.29 ± 0.12 fold, 1.31 ± 0.15 fold, 1.75 ± 0.2 fold, and 2.66 ± 0.2 fold that of the control tissue in the Cur, Cur+M, CM-L, and CM-L+M groups, respectively. The significantly higher regenerated collagen density in the CM-L+M group compared to the control group is especially meaningful, as collagen synthesis is typically slow in patients (particularly those with certain diseases), leading to delayed wound healing. These results suggest that the CM-L+M group effectively promotes collagen deposition in wounds. Additional in vivo experiments are needed to ensure the internal drug toxicity of nanocarriers and microcurrent cloth before entering clinical trials. Identifying drug side effects and drug residues in the body may be further exploration before entering clinical practice.

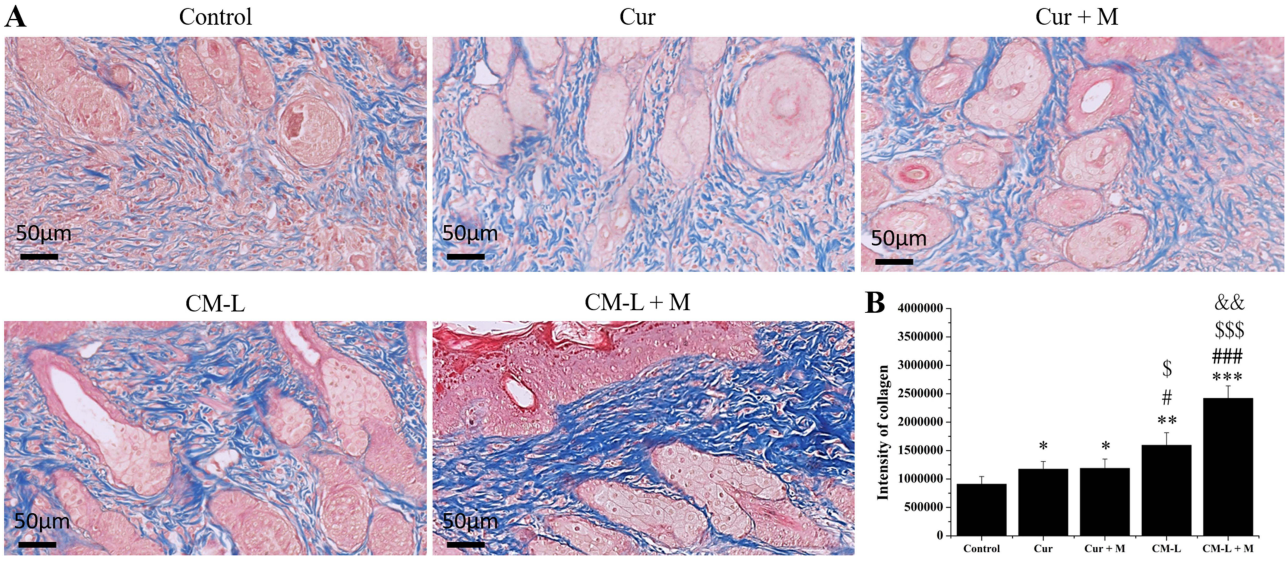

Figure 13 Regenerated collagen matrix of wound sites on day 8 treated with curcumin-loaded micelle formulations and microcurrent cloth. (**A**) Masson's trichrome-stained images (scale bar: 20x, 50 μm). (**B**) Quantified intensity of regenerated collagen matrix. (mean ± SD; *: P < 0.05, **: P< 0.01, ***: P < 0.001 compared with the control; #: P <0.05, ###: P<0.001 compared with Cur; $ < 0.05, $$$< 0.001 compared with Cur + M; andand <0.01 compared with CM-L).

Abbreviations: Cur, free curcumin; Cur+M, free curcumin with microcurrent cloth; CM-L, curcumin-loaded micelles with large particle sizes; CM-L+M, curcumin-loaded micelles with large particle sizes with microcurrent cloth; SD, standard deviation.

Conclusion

Although current drug-delivery systems can solve the problem of the water solubility of poorly soluble ingredients, the particle size of nanoparticles plays a crucial role in transdermal drug delivery routes, especially in barrier-compromised skin. This study thoroughly evaluates the skin penetration ability of microcurrent cloth-assisted Cur-loaded micelles. In vitro characterization showed that the Zn/Ag electrofabric-printed microcurrent cloth had an average potential of +214.6 mV in PBS, which facilitated iontophoretic transdermal delivery of Cur nanoparticles (CM-L) by 20.01-fold increase. Moreover, the localization of CM-L in hair follicles can be altered by microcurrent application, facilitating wound repair process in vivo. Overall, the Zn/Ag electrofabric-printed microcurrent cloth is a promising iontophoretic transdermal drug delivery accelerator, which can promote CMs to cross the barrier of hair follicle and barrier-compromised skin to promote wound healing. Further optimization of electrofabric-printed microcurrent cloth using different metal or metal oxide for the penetration of nanomedicine are necessary to be evaluated for further clinical applications.

Abbreviations

Cur, curcumin; EM, empty micelle; CM, curcumin-loaded micelle; CM-S, curcumin-loaded micelle with small particle size; CM-L, curcumin-loaded micelle with large particle size; Cur+M, free form curcumin with microcurrent cloth; CM-S+M, curcumin-loaded micelle with small particle size with microcurrent cloth; CM-L+M, curcumin-loaded micelle with large particle size with microcurrent cloth; TDD, transdermal drug delivery; PEG, polyethylene glycol 400; DMEM, Dulbecco's modified Eagle's medium; PSN, penicillin–streptomycin-neomycin; FBS, fetal bovine serum; PBS, phosphate-buffered saline; LPS, lipopolysaccharide; SEM, scanning electron microscope; EDX, energy-dispersive X-ray spectroscopy; DLS, dynamic light scattering; HPLC, high-performance liquid chromatography; CLSM, confocal laser scanning microscopy; ELISA, enzyme-linked immunosorbent assay; PDI, polydispersity index; EE, encapsulation efficiency; DL, drug loading; NO, nitric oxide; IL-1β, interleukin-1β; IL-6, interleukin-6; IL-10, interleukin-10; TNF-α, tumor necrosis factor-α; NSAIDs.

Acknowledgments

We thank Jiunn-Wang Liao at the Graduate Institute of Veterinary Pathobiology of National Chung Hsing University for the support of animal studies and the interpretation of the tissue sections.

Disclosure

The authors report no conflicts of interest in this work.

References

1. Zhang Y, Wang S, Yang Y, et al. Scarless wound healing programmed by core-shell microneedles. *Nat Commun*. 2023;14(1):3431. doi:10.1038/s41467-023-39129-6
2. Sun BK, Siprashvili Z, Khavari PA. Advances in skin grafting and treatment of cutaneous wounds. *Science*. 2014;346(6212):941–945. doi:10.1126/science.1253836
3. Talikowska M, Fu X, Lisak G. Application of conducting polymers to wound care and skin tissue engineering: a review. *Biosens. Bioelectron.* 2019;135:50–63. doi:10.1016/j.bios.2019.04.001
4. Raisi A, Asefnejad A, Shahali M, et al. Preparation, characterization, and antibacterial studies of N, O-carboxymethyl chitosan as a wound dressing for bedsore application. *Arch Trauma Res*. 2020;9(4):181–188. doi:10.4103/atr.atr_10_20
5. Eming SA, Wynn TA, Martin P. Inflammation and metabolism in tissue repair and regeneration. *Science*. 2017;356(6342):1026–1030. doi:10.1126/science.aam7928
6. Eming SA, Krieg T, Davidson JM. Inflammation in wound repair: molecular and cellular mechanisms. *J Investigative Dermatol*. 2007;127(3):514–525. doi:10.1038/sj.jid.5700701
7. Kharaziha M, Baidya A, Annabi N. Rational design of immunomodulatory hydrogels for chronic wound healing. *Adv. Mater.* 2021;33(39):2100176. doi:10.1002/adma.202100176
8. Eming SA, Martin P, Tomic-Canic M. Wound repair and regeneration: mechanisms, signaling, and translation. *Sci Translational Med*. 2014;6(265):265sr266. doi:10.1126/scitranslmed.3009337
9. Mu R, Campos de Souza S, Liao Z, Dong L, Wang C. Reprograming the immune niche for skin tissue regeneration – from cellular mechanisms to biomaterials applications. *Adv. Drug Delivery Rev.* 2022;185:114298. doi:10.1016/j.addr.2022.114298
10. Wicke C, Halliday B, Allen D, et al. Effects of steroids and retinoids on wound healing. *Arch Surg*. 2000;135(11):1265–1270. doi:10.1001/archsurg.135.11.1265
11. Guo S, DiPietro LA. Factors affecting wound healing. *J Dental Res*. 2010;89(3):219–229. doi:10.1177/0022034509359125

12. Griffin DR, Archang MM, Kuan C-H, et al. Activating an adaptive immune response from a hydrogel scaffold imparts regenerative wound healing. *Nature Materials*. 2021;20(4):560–569. doi:10.1038/s41563-020-00844-w
13. Qian Y, Zheng Y, Jin J, et al. Immunoregulation in diabetic wound repair with a photoenhanced glycyrrhizic acid hydrogel scaffold. *Adv. Mater.* 2022;34(29):2200521. doi:10.1002/adma.202200521
14. Maschalidi S, Mehrotra P, Keçeli BN, et al. Targeting SLC7A11 improves efferocytosis by dendritic cells and wound healing in diabetes. *Nature*. 2022;606(7915):776–784. doi:10.1038/s41586-022-04754-6
15. Fajgenbaum DC, June CH. Cytokine Storm. *N Eng J Med*. 2020;383(23):2255–2273. doi:10.1056/NEJMra2026131
16. Wang L, Li Y, Xu M, et al. Regulation of inflammatory cytokine storms by mesenchymal stem cells. *Front Immunol*. 2021;12.
17. Wang S, Zheng H, Zhou L, et al. Nanoenzyme-reinforced injectable hydrogel for healing diabetic wounds infected with multidrug resistant bacteria. *Nano Lett*. 2020;20(7):5149–5158. doi:10.1021/acs.nanolett.0c01371
18. Zhou Y, Xie M, Song Y, et al. Two traditional Chinese medicines curcumae radix and curcumae rhizoma: an ethnopharmacology, phytochemistry, and pharmacology review. *Evidence Based Complementary Alternative Med*. 2016;2016:4973128. doi:10.1155/2016/4973128
19. Jurenka JS. Anti-inflammatory properties of curcumin, a major constituent of Curcuma longa: a review of preclinical and clinical research. *Alternative Med Rev*. 2009;14(2):141–153.
20. Peng K-T, Chiang Y-C, Huang T-Y, Chen P-C, Chang P-J, Lee C-W. Curcumin nanoparticles are a promising anti-bacterial and anti-inflammatory agent for treating periprosthetic joint infections. *Int J Nanomed*. 2019;14:469–481. doi:10.2147/IJN.S191504
21. Li S, Yang C, Li J, et al. Progress in pluronic F127 derivatives for application in wound healing and repair. *Int J Nanomed*. 2023;18:4485–4505. doi:10.2147/IJN.S418534
22. Heydari Foroushani P, Rahmani E, Alemzadeh I, et al. Curcumin sustained release with a hybrid chitosan-silk fibroin nanofiber containing silver nanoparticles as a novel highly efficient antibacterial wound dressing. *Nanomaterials*. 2022;12(19):3426. doi:10.3390/nano12193426
23. Ajalli N, Pourmadadi M, Yazdian F, Abdouss M, Rashedi H, Rahdar A. PVA Based Nanofiber Containing GO Modified with Cu Nanoparticles and Loaded Curcumin; High Antibacterial Activity with Acceleration Wound Healing. *J Current Drug Delivery*. 2023;20(10):1569–1583. doi:10.2174/1567201820666221014090334
24. Pourmadadi M, Abbasi P, Eshaghi MM, et al. Curcumin delivery and co-delivery based on nanomaterials as an effective approach for cancer therapy. *J Drug Delivery Sci Technol*. 2022;78:103982. doi:10.1016/j.jddst.2022.103982
25. Kulac M, Aktas C, Tulubas F, et al. The effects of topical treatment with curcumin on burn wound healing in rats. *J Mol Histology*. 2013;44(1):83–90. doi:10.1007/s10735-012-9452-9
26. Shehzad A, Qureshi M, Anwar MN, Lee YS. Multifunctional curcumin mediate multitherapeutic effects. *Journal of Food Science*. 2017;82(9):2006–2015. doi:10.1111/1750-3841.13793
27. Akbik D, Ghadiri M, Chrzanowski W, Rohanizadeh R. Curcumin as a wound healing agent. *Life Sci*. 2014;116(1):1–7. doi:10.1016/j.lfs.2014.08.016
28. Bisht S, Feldmann G, Soni S, et al. Polymeric nanoparticle-encapsulated curcumin ("nanocurcumin"): a novel strategy for human cancer therapy. *J Nanobiotechnol*. 2007;5(1):3. doi:10.1186/1477-3155-5-3
29. Sidhu GS, Mani H, Gaddipati JP, et al. Curcumin enhances wound healing in streptozotocin induced diabetic rats and genetically diabetic mice. *Wound Repair Regeneration*. 1999;7(5):362–374. doi:10.1046/j.1524-475X.1999.00362.x
30. Merrell JG, McLaughlin SW, Tie L, Laurencin CT, Chen AF, Nair LS. Curcumin-loaded poly(epsilon-caprolactone) nanofibres: diabetic wound dressing with anti-oxidant and anti-inflammatory properties. *Clin. Exp. Pharmacol. Physiol.* 2009;36(12):1149–1156. doi:10.1111/j.1440-1681.2009.05216.x
31. Norouzi F, Pourmadadi M, Yazdian F, et al. PVA-based nanofibers containing chitosan modified with graphene oxide and carbon quantum dot-doped TiO2 enhance wound healing in a rat model. *J Funct Biomater*. 2022;13(4):300. doi:10.3390/jfb13040300
32. Liang H, Mirinejad MS, Asefnejad A, et al. Fabrication of tragacanthin gum-carboxymethyl chitosan bio-nanocomposite wound dressing with silver-titanium nanoparticles using freeze-drying method. *Mater Chem Phys*. 2022;279:125770. doi:10.1016/j.matchemphys.2022.125770
33. Raisi A, Asefnejad A, Shahali M, et al. A soft tissue fabricated using a freeze-drying technique with carboxymethyl chitosan and nanoparticles for promoting effects on wound healing. *J Nanoanalysis*. 2020;7(4):262–274.
34. Chen Y, Lu Y, Lee RJ, Xiang G. Nano encapsulated curcumin: and its potential for biomedical applications. *Int J Nanomed*. 2020;15:3099–3120. doi:10.2147/IJN.S210320
35. Li M, Li M, Li X, et al. Preparation, characterization and ex vivo skin permeability evaluation of type I collagen-loaded liposomes. *Int J Nanomed*. 2023;18:1853–1871. doi:10.2147/IJN.S404494
36. Jian YS, Chen CW, Lin CA, et al. Hyaluronic acid-nimesulide conjugates as anticancer drugs against CD44-overexpressing HT-29 colorectal cancer in vitro and in vivo. *Int J Nanomed*. 2017;12:2315–2333. doi:10.2147/IJN.S120847
37. Leung MHM, Colangelo H, Kee TW. Encapsulation of curcumin in cationic micelles suppresses alkaline hydrolysis. *Langmuir*. 2008;24(11):5672–5675. doi:10.1021/la800780w
38. He C, Hu Y, Yin L, Tang C, Yin C. Effects of particle size and surface charge on cellular uptake and biodistribution of polymeric nanoparticles. *Biomaterials*. 2010;31(13):3657–3666. doi:10.1016/j.biomaterials.2010.01.065
39. Lu F, Wu SH, Hung Y, Mou CY. Size effect on cell uptake in well-suspended, uniform mesoporous silica nanoparticles. *Small*. 2009;5(12):1408–1413. doi:10.1002/smll.200900005
40. Shim J, Seok Kang H, Park W-S, Han S-H, Kim J, Chang I-S. Transdermal delivery of minoxidil with block copolymer nanoparticles. *J Control Release*. 2004;97(3):477–484. doi:10.1016/S0168-3659(04)00167-1
41. Knorr F, Lademann J, Patzelt A, Sterry W, Blume-Peytavi U, Vogt A. Follicular transport route – research progress and future perspectives. *Eur. J. Pharm. Biopharm.* 2009;71(2):173–180. doi:10.1016/j.ejpb.2008.11.001
42. Ita K. Transdermal delivery of heparin: physical enhancement techniques. *Int J Pharm*. 2015;496(2):240–249. doi:10.1016/j.ijpharm.2015.11.023
43. Yang R, Wei T, Goldberg H, Wang W, Cullion K, Kohane DS. Getting drugs across biological barriers. *Adv. Mater.* 2017;29(37). doi:10.1002/adma.201606596
44. Poltawski L, Watson T. Bioelectricity and microcurrent therapy for tissue healing – a narrative review. *Phys Therapy Rev*. 2009;14(2):104–114. doi:10.1179/174328809X405973

45. Ita K. Transdermal iontophoretic drug delivery: advances and challenges. *J Drug Targeting*. 2016;24(5):386–391. doi:10.3109/1061186X.2015.1090442
46. Dowlatababdi FH, Amiri G, Mohammadi Sichani MJNJ. Investigation of the antimicrobial effect of silver doped Zinc Oxide nanoparticles. *Nanomedicine J*. 2017;4(1):50–54.
47. Xiao X, Liu E, Shao J, Ge S. Advances on biodegradable zinc-silver-based alloys for biomedical applications. *J Appl Biomaterials Functional Materials*. 2021;19:22808000211062407. doi:10.1177/22808000211062407
48. Chae JS, Park SK, Roh KC, Park HS. Electrode materials for biomedical patchable and implantable energy storage devices. *Energy Storage Mater.* 2020;24:113–128. doi:10.1016/j.ensm.2019.04.032
49. Park H-K, Kong B-S, E-S O. Effect of high adhesive polyvinyl alcohol binder on the anodes of lithium ion batteries. *Electrochem. Commun.* 2011;13(10):1051–1053. doi:10.1016/j.elecom.2011.06.034
50. Chaouat M, Le Visage C, Baille WE, et al. A novel cross-linked poly(vinyl alcohol) (PVA) for vascular grafts. *Adv Funct Mater*. 2008;18(19):2855–2861. doi:10.1002/adfm.200701261
51. Fan L, Guo Z, Zhang Y, et al. Stable artificial solid electrolyte interphase films for lithium metal anode via metal–organic frameworks cemented by polyvinyl alcohol. *J Mater Chem A*. 2020;8(1):251–258. doi:10.1039/C9TA10405D
52. Li C-Z, Chang H-M, Hsu W-L, Venkatesan P, Lin MH-C, Lai P-S. Curcumin-loaded oil-free self-assembled micelles inhibit the influenza a virus activity and the solidification of curcumin-loaded micelles for pharmaceutical applications. *Pharmaceutics*. 2022;14(11):2422. doi:10.3390/pharmaceutics14112422
53. Ternullo S, Basnet P, Holsæter AM, Flaten GE, de Weerd L, Škalko-basnet N. Deformable liposomes for skin therapy with human epidermal growth factor: the effect of liposomal surface charge. *Eur. J. Pharm. Sci.* 2018;125:163–171. doi:10.1016/j.ejps.2018.10.005
54. Sarika P, James NR, Raj DK. Galactosylated alginate-curcumin micelles for enhanced delivery of curcumin to hepatocytes. *Int J Biol Macromol*. 2016;86:1–9. doi:10.1016/j.ijbiomac.2016.01.037
55. Song L, Shen Y, Hou J, Lei L, Guo S, Qian C. Polymeric micelles for parenteral delivery of curcumin: preparation, characterization and in vitro evaluation. *Colloids Surf., A*. 2011;390(1):25–32. doi:10.1016/j.colsurfa.2011.08.031
56. Abdel-Hafez SM, Hathout RM, Sammour OA. Curcumin-loaded ultradeformable nanovesicles as a potential delivery system for breast cancer therapy. *Colloids Surf., B*. 2018;167:63–72. doi:10.1016/j.colsurfb.2018.03.051
57. Danafar H, Davaran S, Rostamizadeh K, Valizadeh H, Hamidi M. Biodegradable m-PEG/PCL core-shell micelles: preparation and characterization as a sustained release formulation for curcumin. *Adv Pharm Bulletin*. 2014;4(Suppl 2):501–510. doi:10.5681/apb.2014.074
58. Jahed V, Zarrabi A, Bordbar A-K, Hafezi MS. NMR (1H, ROESY) spectroscopic and molecular modelling investigations of supramolecular complex of β-cyclodextrin and curcumin. *Food Chem*. 2014;165:241–246. doi:10.1016/j.foodchem.2014.05.094
59. Esmaili M, Ghaffari SM, Moosavi-Movahedi Z, et al. Beta casein-micelle as a nano vehicle for solubility enhancement of curcumin; food industry application. *LWT Food Sci Technol*. 2011;44(10):2166–2172. doi:10.1016/j.lwt.2011.05.023
60. Nair RS, Morris A, Billa N, Leong C-O. An evaluation of curcumin-encapsulated chitosan nanoparticles for transdermal delivery. *AAPS PharmSciTech*. 2019;20(2):69. doi:10.1208/s12249-018-1279-6
61. Bae I-H, Park JW, Kim D-Y. Enhanced regenerative healing efficacy of a highly skin-permeable growth factor nanocomplex in a full-thickness excisional mouse wound model. *Int J Nanomed*. 2014;9:4551–4567. doi:10.2147/IJN.S68399
62. Wang X, Huang H, Chu X, et al. Encapsulation and binding properties of curcumin in zein particles stabilized by Tween 20. *Colloids Surf., A*. 2019;577:274–280. doi:10.1016/j.colsurfa.2019.05.094
63. Chen Y-S, Chiu Y-H, Y-S L, et al. Integration of PEG 400 into a self-nanoemulsifying drug delivery system improves drug loading capacity and nasal mucosa permeability and prolongs the survival of rats with malignant brain tumors. *Int J Nanomed*. 2019;14:3601–3613. doi:10.2147/IJN.S193617
64. Zhang P, Peng X, Araki Y, et al. Fabrication of a CuZn-based catalyst using a polyethylene glycol surfactant and supercritical drying. *Catal Sci Technol*. 2020;10(24):8410–8420. doi:10.1039/D0CY00961J
65. Kurien BT, Matsumoto H, Scofield RH. Nutraceutical value of pure curcumin. *J Pharm Magazine*. 2017;13(Suppl 1):67.
66. Liu Y, Yang G, Jin S, Xu L, Zhao C-X. Development of high-drug-loading nanoparticles. *ChemPlusChem*. 2020;85(9):2143–2157. doi:10.1002/cplu.202000496
67. Mendes C, Thirupathi A, Zaccaron RP, et al. Microcurrent and gold nanoparticles combined with hyaluronic acid accelerates wound healing. *Antioxidants*. 2022;11(11):2257. doi:10.3390/antiox11112257
68. Cui LL, Hou XM, Jiang J, Li GD, Liang YY, Xin X. Comparative enhancing effects of electret with chemical enhancers on transdermal delivery of meloxicam in vitro. *J Phys Conf Ser.* 2008;142(1):012015.
69. Lin C-A, H-M H, Venkatesan P, et al. Hyaluronic acid-glycine-cholesterol conjugate-based nanoemulsion as a potent vaccine adjuvant for T cell-mediated immunity. *Pharmaceutics*. 2021;13(10):1569. doi:10.3390/pharmaceutics13101569
70. Maiti K, Mukherjee K, Gantait A, Saha BP, Mukherjee PK. Curcumin–phospholipid complex: preparation, therapeutic evaluation and pharmacokinetic study in rats. *Int J Pharm*. 2007;330(1):155–163. doi:10.1016/j.ijpharm.2006.09.025
71. Fortunato AK, Pontes WM, De Souza DMS, et al. Strength training session induces important changes on physiological, immunological, and inflammatory biomarkers. *J Immunol Res*. 2018;2018:9675216. doi:10.1155/2018/9675216
72. Bisht K, Choi WH, Park SY, Chung MK, Koh WS. Curcumin enhances non-inflammatory phagocytic activity of RAW264.7 cells. *Biochem. Biophys. Res. Commun.* 2009;379(2):632–636. doi:10.1016/j.bbrc.2008.12.135
73. Korelo RI, Kryczyk M, Garcia C, Naliwaiko K, Fernandes LC. Wound healing treatment by high frequency ultrasound, microcurrent, and combined therapy modifies the immune response in rats. *J Brazilian J Phys Therapy*. 2016;20:133–141. doi:10.1590/bjpt-rbf.2014.0141
74. Gouthamchandra K, Sudeep HV, Chandrappa S, Raj A, Naveen P, Shyamaprasad K. Efficacy of a standardized turmeric extract comprised of 70% bisdemothoxy-curcumin (REVERC3) against LPS-induced inflammation in RAW264.7 cells and carrageenan-induced paw edema. *J Inflammation Res*. 2021;14:859–868. doi:10.2147/JIR.S291293
75. Aguayo-Morales H, Sierra-Rivera CA, Claudio-Rizo JA, Cobos-Puc LE. Horsetail (equisetum hyemale) extract accelerates wound healing in diabetic rats by modulating IL-10 and MCP-1 release and collagen synthesis. *Pharmaceuticals*. 2023;16(4):514. doi:10.3390/ph16040514
76. Johnson BZ, Stevenson AW, Prêle CM, Fear MW, Wood FM. The role of IL-6 in skin fibrosis and cutaneous wound healing. *Biomedicines*. 2020;8(5):101. doi:10.3390/biomedicines8050101

77. Uchida T, Kadhum WR, Kanai S, Todo H, Oshizaka T, Sugibayashi K. Prediction of skin permeation by chemical compounds using the artificial membrane, Strat-M™. *Eur. J. Pharm. Sci.* 2015;67:113–118. doi:10.1016/j.ejps.2014.11.002
78. Tiyaboonchai W, Tungpradit W, Plianbangchang P. Formulation and characterization of curcuminoids loaded solid lipid nanoparticles. *Int J Pharm*. 2007;337(1):299–306. doi:10.1016/j.ijpharm.2006.12.043
79. Sartorelli P, Andersen HR, Angerer J, et al. Percutaneous penetration studies for risk assessment. *Environ. Toxicol. Pharmacol.* 2000;8(2):133–152. doi:10.1016/S1382-6689(00)00035-1
80. Ruela ALM, Perissinato AG, MEdS L, Mudrik PS, Pereira GR. Evaluation of skin absorption of drugs from topical and transdermal formulations. *Br J Pharm Sci*. 2016;52(3):527–544. doi:10.1590/s1984-82502016000300018
81. Mohanty C, Sahoo SK. Curcumin and its topical formulations for wound healing applications. *Drug Discovery Today*. 2017;22(10):1582–1592. doi:10.1016/j.drudis.2017.07.001
82. Yu C, Xu Z-Z, Hao Y-H, et al. A novel microcurrent dressing for wound healing in a rat skin defect model. *Military Med Res*. 2019;6(1):22. doi:10.1186/s40779-019-0213-x
83. Nair HKR. Microcurrent as an adjunct therapy to accelerate chronic wound healing and reduce patient pain. *J Wound Care*. 2018;27(5):296–306. doi:10.12968/jowc.2018.27.5.296
84. Bhattacharya D, Ghosh B, Mukhopadhyay M. Development of nanotechnology for advancement and application in wound healing: a review. *IET Nanobiotechnol*. 2019;13(8):778–785. doi:10.1049/iet-nbt.2018.5312
85. Ahmadian Z, Gheybi H, Adeli M. Efficient wound healing by antibacterial property: advances and trends of hydrogels, hydrogel-metal NP composites and photothermal therapy platforms. *J Drug Delivery Sci Technol*. 2022;73:103458. doi:10.1016/j.jddst.2022.103458
86. Mirzahosseinipour M, Khorsandi K, Hosseinzadeh R, Ghazaeian M, Shahidi FK. Antimicrobial photodynamic and wound healing activity of curcumin encapsulated in silica nanoparticles. *Photodiagnosis Photodynamic Therapy*. 2020;29:101639. doi:10.1016/j.pdpdt.2019.101639
87. Liang Y, Chen B, Li M, He J, Yin Z, Guo B. Injectable antimicrobial conductive hydrogels for wound disinfection and infectious wound healing. *Biomacromolecules*. 2020;21(5):1841–1852. doi:10.1021/acs.biomac.9b01732
88. Long L, Hu C, Liu W, et al. Injectable multifunctional hyaluronic acid/methylcellulose hydrogels for chronic wounds repairing. *Carbohydr Polym*. 2022;289:119456. doi:10.1016/j.carbpol.2022.119456
89. Rao SS, Prabhu A, Kudkuli J, Surya S, Rekha PD. Hyaluronic acid sustains platelet stability with prolonged growth factor release and accelerates wound healing by enhancing proliferation and collagen deposition in diabetic mice. *J Drug Delivery Sci Technol*. 2022;67:102898. doi:10.1016/j.jddst.2021.102898
90. Krausz AE, Adler BL, Cabral V, et al. Curcumin-encapsulated nanoparticles as innovative antimicrobial and wound healing agent. *Nanomedicine*. 2015;11(1):195–206. doi:10.1016/j.nano.2014.09.004
91. Gnanasambanthan HG, Maji D. Development of a flexible and wearable microelectrode array patch using a screen-printed masking technique for accelerated wound healing. *ACS Applied Electronic Materials*. 2023;5(8):4426–4436. doi:10.1021/acsaelm.3c00637
92. Chen Y, Xu W, Zheng X, et al. Two-layered biomimetic flexible self-powered electrical stimulator for promoting wound healing. *Biomacromolecules*. 2023;24(3):1483–1496. doi:10.1021/acs.biomac.2c01520
93. Cheah YJ, Buyong MR, Mohd Yunus MH. Wound healing with electrical stimulation technologies: a review. *Polymers*. 2021;13(21):3790. doi:10.3390/polym13213790